AD-A073 467 CORNELL UNIV ITHACA N Y LAB OF PLASMA STUDIES F/G 4/1
TEMPORAL AND SPATIAL POWER SPECTRUM STUDIES OF NUMERICAL SIMULA--ETC(U)
JUN 78 M J KESKINEN, R N SUDAN, R L FERCH N00173-77-C-0240
UNCLASSIFIED LPS-243 NL

| OF |
AD
A073487

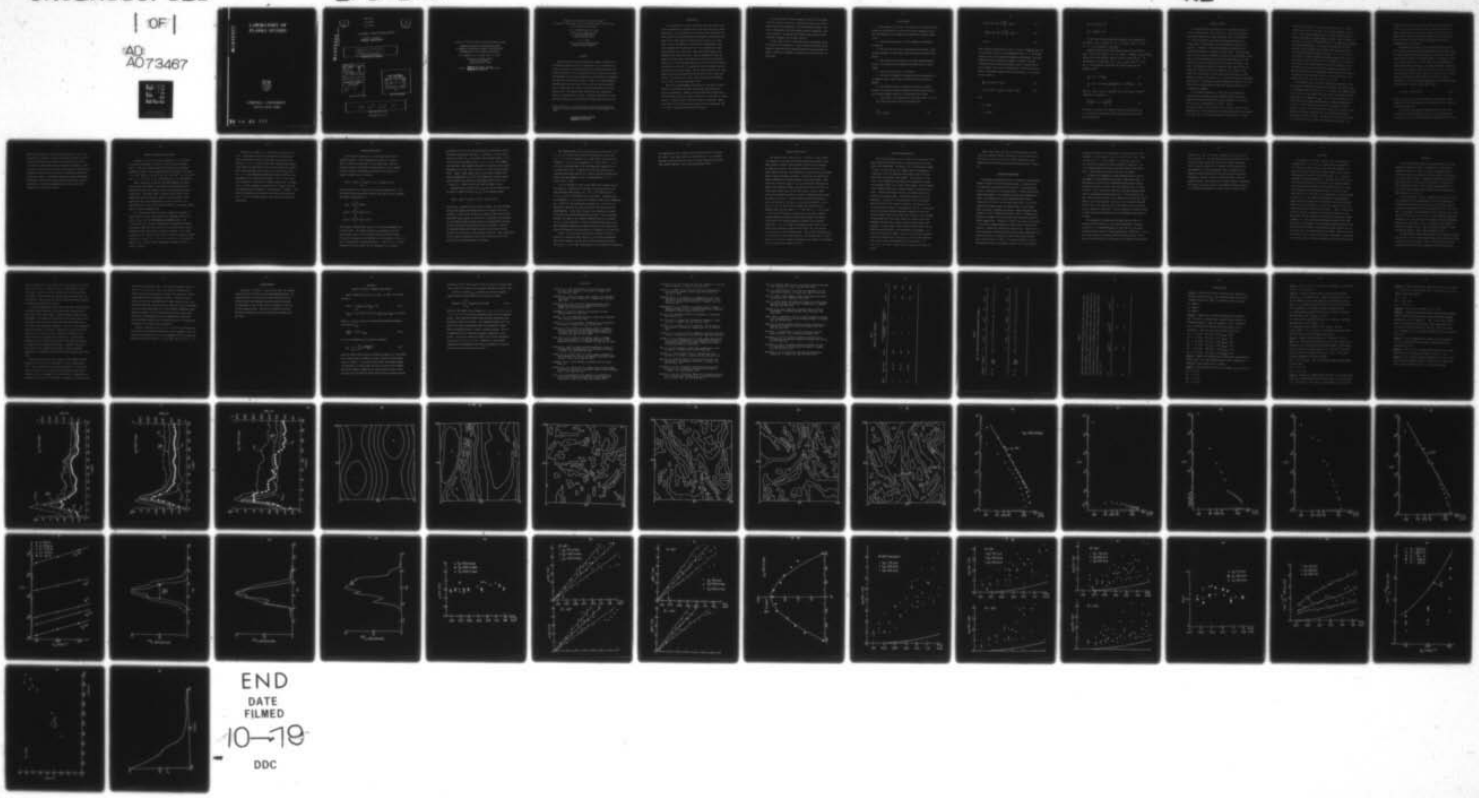

END
DATE
FILMED
10-79
DDC

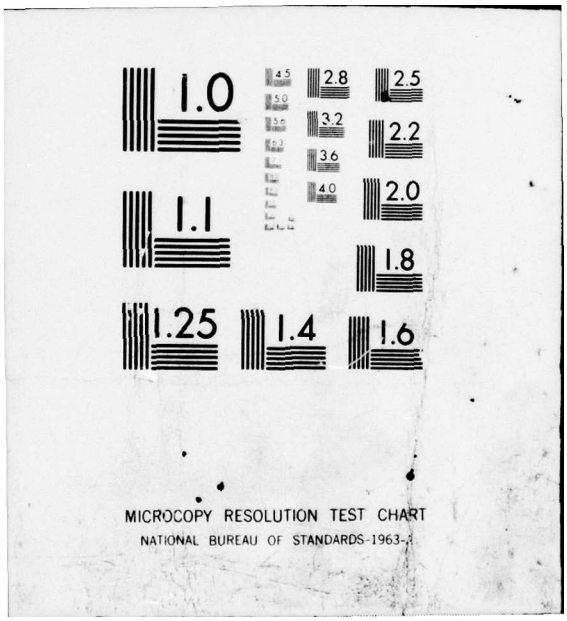
1.0
1.1
1.25
1.4
1.6
1.8
2.0
2.2
2.5
2.8
3.2
3.6
4.0
4.5
5.0
MICROCOPY RESOLUTION TEST CHART
NATIONAL BUREAU OF STANDARDS-1963-

AD A073467

LABORATORY OF PLASMA STUDIES

CORNELL UNIVERSITY

ITHACA, NEW YORK

79 08 23 101

DATA SHEET

PHOTOGRAPH

THIS SHEET

II
LEVEL

1
INVENTORY

AD A073467
DDC-ACCESSION NUMBER

Cornell Univ - Lab of Plasma Studies

LPS-243
DOCUMENT IDENTIFICATION

DISTRIBUTION STATEMENT A
Approved for public release;
Distribution Unlimited
DISTRIBUTION STATEMENT

Accession For
NTIS GRA&I [X]
DDC TAB [ ]
Unannounced [ ]
Justification per Doc.
By
Distribution/
Availability Codes
Dist | Avail and/or special
A
DISTRIBUTION STAMP

DDC
RECEIVED
SEP 5 1979
E
DATE ACCESSIONED

79 08 23 101
DATE RECEIVED IN DDC

PHOTOGRAPH THIS COPY

Contract N 00173-77-C-0240, monitored by NRL code 6700

Temporal and Spatial Power Spectrum Studies of Numerical Simulations of Type II Gradient Drift Irregularities in the Equatorial Electrojet

M. J. Keskinen, R. N. Sudan, and R. L. Ferch

Laboratory of Plasma Studies
Cornell University
Ithaca, New York 14853

LPS 243

APPROVED FOR PUBLIC RELEASE
DISTRIBUTION UNLIMITED

June 1978

Temporal and Spatial Power Spectrum Studies of Numerical Simulations of Type II Gradient Drift Irregularities in the Equatorial Electrojet

M. J. Keskinen[†] and R. N. Sudan

Laboratory of Plasma Studies
Cornell University
Ithaca, New York 14853

R. L. Ferch

Atomic Energy of Canada Limited
Pinawa, Manitoba, Canada

ABSTRACT

Temporal and spatial power spectra from computer simulations of the equations modeling Type II irregularities in the equatorial electrojet are presented. The power spectra are computed using the code of Ferch and Sudan (1977), averaging over times as long as 20 seconds. The dependence of the average frequencies and linewidths on wavelength and angle from the electrojet drift is studied. The mean frequencies obtained agree well with linear theory except at short wavelengths while the linewidths are greater than those predicted by the linear damping rates. The spatial power spectra were also computed and found to be approximately isotropic. Favorable comparisons are made with radar observations and the theory of Sudan and Keskinen (1977).

[†]Present affiliation: National Research Council Resident Research Associate at Naval Research Laboratory, Code 7750, Washington, D.C. 20375

APPROVED FOR PUBLIC RELEASE
DISTRIBUTION UNLIMITED

INTRODUCTION

In the equatorial E region, radar backscatter observations have shown irregularities in plasma density whose spectral width is often comparable to the mean Doppler shift and whose phase velocities are on the order of the electron drift speed [Balsley, 1969; Balsley and Farley, 1971, 1973; Farley and Balsley, 1973; Fejer et al., 1975, 1976]. Many of the features of these Type II irregularities have been explained with the linear theory of the gradient drift instability [Maeda et al., 1963; Knox, 1964; Reid, 1968; Rogister and D'Angelo, 1970; Whitehead, 1971]. Both one-dimensional [Sato and Tsuda, 1967; Sato, 1971, 1973; Rogister, 1972] and two-dimensional [Sudan et al., 1973] nonlinear theories have been proposed to explain the presence of the Type II irregularities with wavelengths that are predicted to be linearly damped. The two-dimensional model has found support both from experiment [Balsley and Farley, 1973; Farley and Balsley, 1973; Fejer et al., 1975, 1976] and simulation [McDonald et al., 1974, 1975; Ferch and Sudan, 1977].

Much of our understanding of the physics of the Type II irregularities is based upon VHF radar observations, particularly the spectral measurements. However, existing radars have studied only a few wavelengths whereas the range of scale sizes of the Type II irregularities is known to span at least two orders of magnitude. Spectra from numerical simulations can be computed for many wavelengths and, as a result, supplement experimental observation.

We have extended a previous numerical study [Ferch and Sudan, 1977] and, using the same code, computed the temporal and spatial power spectra from simulations of the two-dimensional model. This code is sufficiently fast that moderate spectral integration times can be achieved. The numerically obtained temporal power spectra favorably reproduces Type II radar spectra.

In this paper we first review the linear and nonlinear theory of the Type II irregularities. Then we present the results of the numerical simulations while making comparisons with experiment and theory. Finally we summarize and discuss the principal results of this study.

LINEAR THEORY

For wavelengths of more than a few meters, the E region electrojet plasma can be described as an electron and singly charged ion fluid. The fluid equation can be simplified by making the following assumptions:

1. The electron gyroradius is small compared to wavelengths of interest.

2. The wave electric field is essentially electrostatic, since the plasma pressure is much smaller than the ambient magnetic energy density.

3. The electron and ion densities are equal (quasineutrality) since we are interested in wavelengths much larger than the Debye length.

4. The ions and electrons are isothermal.

5. The waves are assumed to propagate exactly perpendicular to the magnetic field, since these waves suffer the least diffusive damping.

6. The electron inertia is neglected, because the electron-neutral collision and cyclotron frequencies are much larger than the wave frequency Doppler-shifted to the electrojet drift frame.

7. Ion inertia is also neglected for the same reasons as in (6).

With these restrictions the fluid equations are:

$$\frac{\partial n_\alpha}{\partial t} + \nabla \cdot n_\alpha \underset{\sim}{v}_\alpha = 0 \qquad (1)$$

$$\frac{e}{m_e}(\underset{\sim}{E} + \underset{\sim}{V}_e \times \underset{\sim}{B}) + u_e^2 \frac{\nabla n_e}{n_e} + \nu_e \underset{\sim}{V}_e = 0 \tag{2}$$

$$-\frac{Ze}{m_i}(\underset{\sim}{E} + \underset{\sim}{V}_i \times \underset{\sim}{B}) + n_i^2 \frac{\nabla n_i}{n_i} + \nu_i \underset{\sim}{V}_i = 0 \tag{3}$$

$$\nabla \cdot \underset{\sim}{J} = 0 \tag{4}$$

where α denotes electrons (e) or ions (i) and $\underset{\sim}{J} = ne(Z\underset{\sim}{V}_i - \underset{\sim}{V}_e)$, $\underset{\sim}{E} = -\nabla\phi$ is the electric field, B is the geomagnetic field, u, is the thermal velocity, and ν is the collision frequency with neutrals. All other symbols have their conventional meaning. We adopt a Cartesian coordinate system in which the magnetic field is aligned with the x axis (north), the y axis is westward, and z direction vertically upward. Eliminating algebraically the velocities V_e, V_i, equations (1)-(4) reduce to

$$\frac{\partial n}{\partial t} + \mu_a \hat{x} \times \nabla\phi \cdot \nabla n = D_a \nabla^2 n \tag{5}$$

$$\beta\mu_a \hat{x} \times \nabla\phi \cdot \nabla n + \mu_a(\nabla\phi \cdot \nabla n + n\nabla^2\phi) = D'\nabla^2 n \tag{6}$$

where

$$\Omega_e = eB/m_e$$

$$\Omega_i = ZeB/m_i$$

$$\mu_H^e = e\Omega_e/m_e(\Omega_e^2 + \nu_e^2)$$

$$D_\perp^i = \nu_i U_i^2/(\Omega_i^2 + \nu_i^2)$$

In the lower E region equatorial electrojet, the parameters are such that $\beta \simeq (1 + \psi)^{-1}\nu_i/\Omega_i$, $\mu_a \simeq (1 + \psi)^{-1}\mu_H^e$, $D_a \simeq 2\psi(1 + \psi)^{-1}D_\perp^i$, $D' \simeq (1 + \psi)^{-2}(\nu_i/\Omega_i)D_\perp^i$, $\psi \equiv \nu_e\nu_i/\Omega_e\Omega_i$.

Equations (5) and (6) can be linearized about the equilibrium $n_o(z) = N_o(1 + z/L)$, $d\phi_o/dz = a(z + L)^{-1}$ where $a = B(V_d^2/\Omega_e - (1+(\nu_e/\Omega_e)^2)LV_d]$ and V_d is the electron drift velocity (in the y direction) at $z = 0$. Fluctuations $n = \tilde{n}\exp\{i[k_y y + k_z z - (\omega_{kr} + i\gamma_k)t]\}$ with $k\cdot B = 0$ and $k_y L >> 1$ have frequency and growth rate given by [Rogister and D'Angelo, 1970]

$$\underset{\sim}{\omega_{kr}} \equiv (1 + \psi)^{-1}\,\underset{\sim}{k}\cdot\underset{\sim}{V_d} \tag{7}$$

$$\underset{\sim}{\gamma_k} = [\psi(1 + \psi)^{-1}]\{(\Omega_e/\nu_e)[k_y^2 V_d/k^2 L(1 + \psi)] - k^2 C_s^2/\nu_i\} \tag{8}$$

where $C_s^2 = K(T_e + T_i)/m_i = (m_e/m_i)n_e^2 + n_i^2$ is the acoustic velocity. Instability is possible if

$$\frac{V_d}{L}\left(\frac{k_y}{k}\right)^2 > (1 + \psi)\,\frac{\gamma_e}{\Omega_e}\,\frac{k^2 C_s^2}{\nu_i} \tag{9}$$

Note that L is positive for density increasing with altitude and V_d is positive for electrons drifting toward the west, the usual daytime conditions.

NONLINEAR THEORY

The minimum unstable wavelength for the ionospheric parameters of the E-region from Eq. (9) is about 30 m. The radar backscatter observations indicate very large nonthermal density fluctuations at 3 m. These fluctuations are stable and damped according to the linear theory of the previous section and therefore should not be excited. In addition, vertically propagating irregularities are observed that cannot be accounted by linear theory. The explanation lies in the fact that the unstable oscillations with wavelengths longer than 30 m couple nonlinearly to these short wavelengths and in the steady state the rate of excitation just balances the damping. However, one dimensional theories of nonlinear wave coupling [Sato and Tsuda, 1967; Tsuda and Sato, 1967; Rogister, 1972] cannot explain either the vertical Type II radar echoes [Farley and Balsley, 1973; Balsley and Farley, 1973; Fejer et al., 1976] or the density fluctuation amplitudes of 2-5% observed in rocket experiments [Prakash et al. 1969, 1970, 1972] for weak electrojet conditions when presumably Type II irregularities dominate.

It was shown by Sudan et al. (1969) that a one dimensional nonlinear wave steepening requires abnormally large fluctuating amplitudes 30-50% and therefore the actual mechanism for such interaction must be two-dimensional in nature. Since the group velocity of all the waves is the same viz. $V_d/(1 + \psi)$ the wavepackets can couple strongly to each other because they stay together for a long time. In the frame moving with velocity $V_d/(1 + \psi)$ with

respect to the laboratory an unstable wave appears to be a purely growing wave since the real part of the frequency doppler shifts to zero. A horizontally propagating wave will have local horizontal density and potential gradients $d\tilde{n}/dy$ and $d\tilde{\phi}/dy$. Where the phase of the wave is such that $(dn^{(1)}/dy)d\phi^{(1)}/dy > 0$, secondary short wavelength oscillation propagating in the vertical direction will be driven unstable in exact analogy to the primary waves driven unstable by the equilibrium gradients $(dn_o/dz)\ (d\phi_o/dz) > 0$. In this manner it is possible to generate shorter wavelength secondary waves and it is also evident that the spectrum of these secondary waves is likely to be isotropic in the plane transverse to the static magnetic field. This theory can account for vertically propagating irregularities and also predicted the two-dimensional turbulent nature of the Type II irregularities experimentally verified by Farley and Balsley, 1973; Balsley and Farley, 1973 and by Fejer et al., 1976.

The frequency spectra of the 3 m fluctuations measured by radar backscattering techniques indicate that the peak of the spectra occurs at a frequency which is given by Eq. (7). However, the frequency width of the spectra is much larger than that given by the damping rate (8) and indeed it is comparable to $\omega_{\underset{\sim}{k}r}$. This is also indicative of the strong interaction between waves leading to a nonlinear damping far in excess of linear damping rate and may be explained as follows. Suppose we launch a test wave with wave vector $\underset{\sim}{k}$ into a region of well developed turbulence containing waves of all possible wavelengths propagating in every direction. The test wave will immediately couple to two other waves, $\underset{\sim}{k}'$, $\underset{\sim}{k}''$ whose wave numbers satisfy $\underset{\sim}{k} = \underset{\sim}{k}' + \underset{\sim}{k}''$,

because the phase variation of the test wave will be synchronized to the vector sum of the other two waves. Because the waves are almost dispersionless and the group velocity of all the waves is approximately equal such interaction could occur over a long time and the transfer of energy from $\underset{\sim}{k}$ to $\underset{\sim}{k}'$ and $\underset{\sim}{k}''$ would result in rapid damping of the test wave.

The quantitative analysis of the nonlinear effects described above has been undertaken by Sudan and Keskinen (1977) using a theory of strong turbulence whose basic premise is the "direct interaction approximation" pioneered by Kraichnan (1959). The principal results of this investigation are: (1) The steady state two dimensional density fluctuation spectrum I_k is isotropic and follows a power law k^{-n} where n lies between 2 and 4, but is closer to 3.2 if one accepts radar data which shows that $I_k = V_d^2$ at 3 m. The mean r.m.s. density fluctuation predicted by this theory falls within the range of observations. (2) The nonlinear damping rate or the frequency width of the spectrum is given by $(\gamma_k^2 + \Gamma_k^2)^{1/2}$ where,

$$\Gamma_k = \text{const.} \times \beta V_d k^2 I_k^{1/2} \tag{10}$$

where $\beta = \nu_i/\Omega_i(1 + \psi)$ and the constant is of order unity. This expression is verified against radar observations and the simulation results presented later.

On the other hand, Rognlien and Weinstock (1973, 1974) have estimated the saturated amplitude of large scale gradient-drift fluctuations using the nonlinear theory of perturbed particle orbits

[Weinstock and Williams, 1971; Sleeper and Weinstock, 1972]. The perturbed orbit theory is based on the supposition that an excited spectrum of incoherent waves causes the stochastic diffusion of collisionless orbits which leads to nonlinear wave damping. Since the ions are collisional this concept cannot apply to them while the magnitude of this effect on electrons is insignificant because the electron gyroradius is negligible compared to unstable wavelengths. Furthermore, such theories cannot explain the generation of short wavelength or vertically propagating waves since explicit mode coupling is not taken into account.

NUMERICAL SIMULATIONS AND RESULTS

Equations (5) and (6) were solved numerically. A description of the code and methods of solution is given in Ferch and Sudan (1977). With the exception of the drift velocity, V_d, identical parameters, typical of the daytime equatorial electrojet, were used: $B = 3 \times 10^{-5}$ W/m^2, $\Omega_i = 96$ sec^{-1}, $\Omega_e = 5.3 \times 10^6$ sec^{-1}, $\nu_i = 2.5 \times 10^3$ sec^{-1}, $\nu_e = 4 \times 10^4$ sec^{-1}, $u_i^2 = 10^5$ m^2/sec^2, $u_e^2 = 5.5 \times 10^9$ m^2/sec^2.

Table 1 summarizes the models from which temporal and spatial power spectra were computed. Each model was initialized with an unstable horizontal wave together with a smaller amplitude vertical perturbation. All models could be advanced in time until a quasi-steady state had been achieved. Model 1, the most weakly driven, required the most time (approximately 32 sec) to saturate. All three models were run on a CDC 7600, with Model 1, for example, taking about 1.5 hours of computer time.

As t increased the region of nonzero $|\delta n(\underset{\sim}{k},t)|^2$ cascaded to larger values of $(k_y/k_o, k_z/k_o)$ than those originally excited (1,0) and (0,1); $k_o = 2\pi/L$ is the fundamental wavenumber and L = 128 is the system size. The time evolution of the maximum total density fluctuation, amplitude of the initial 128 m horizontal wave, and the maximum horizontal and vertical velocities for Models 1-3 are shown in Figures 1a-1c. Density contour plots for Model 3, the most strongly driven (V_d = 125 m/s), at t = 0, 2, 4, 12, 26, 34 sec are displayed in Figures 2a-2f. Density contour development for Models 1 and 2 is similar to Model 3.

The behavior of Model 3 is illustrated in Figure 1e-1f and 2a-2f. The maximum total density fluctuation and maximum horizontal and vertical velocities, which peak in an earlier time interval, t = 3-5 sec, than the other less strongly driven models, attain values of approximately 14.8%, 425 m/s and 300 m/s, respectively, whereupon they relax and describe a quasi-steady state. By t = 1 sec, the maximum horizontal and vertical velocities were comparable to the original drift velocity. At t = 2 sec, small scale turbulence is seen from the density contour plot. In Models 1 and 2, similar behavior is observed but on a longer time scale with smaller density fluctuations and velocities. In Model 1, the density fluctuations and horizontal and vertical velocities peak near t = 6-8 sec reaching values of 11.8%, 250 m/s, and 200 m/s, respectively.

SPATIAL POWER SPECTRA

Let the spatial power spectra in the quasi-steady state be defined as $I(\underset{\sim}{k},t) = (L/2\pi)^2 \langle |\delta n(\underset{\sim}{k},t)/n_o|^2 \rangle$ where $\delta n = n - n_o(z)$ and L^2 is the area of the mesh. In the quasi-steady state the ensemble average is understood to be equivalent to a time average. In order to analyze the degree of isotropy of the spectrum, we expand in Fourier series as follows,

$$I(k,t) = I(k,t) + \sum_{n=1}^{N} (f_n(k,t) \cos n\theta + g_n(\underset{\sim}{k},t) \sin n\theta)$$

where the sum over n is restricted to positive integers and $k = |k|$. Box normalization and periodic boundary conditions have been employed. The Fourier coefficients are

$$I(k,t) = \frac{1}{2\pi} \int_0^{2\pi} d\theta \; I(\underset{\sim}{k},t)$$

$$f_n(k,t) = \frac{1}{\pi} \int_0^{2\pi} d\theta \; I(\underset{\sim}{k},t) \cos n\theta$$

$$g_n(k,t) = \frac{1}{\pi} \int_0^{2\pi} d\theta \; I(\underset{\sim}{k},t) \sin n\theta$$

From symmetry considerations ($\delta n(y,z,t)$ real) the odd-numbered coefficients vanish. The angular integrals are computed in discrete (k_y,k_z) space using a block-integration nearest grid-point scheme. The $f_n(k,t)$ and $g_n(k,t)$ were evaluated for k in the range $1 \leq k/k_o \leq 14$. This is equivalent to a wavelength regime $\lambda = 2\pi/k$ of $9 \text{ m} \lesssim \lambda \lesssim 128 \text{ m}$. Although in all three models the cell spacing was 2 m, spectral

information for $\lambda \lesssim 9$ m was disregarded due to insufficient spatial resolution and aliasing limitations. Initially, a 15-term fitting function was used, i.e., an isotropic term and equal numbers (7) of sin $n\theta$ and cos $n\theta$ harmonics with $n = 2, 4, \ldots, 14$. Equal numbers were used due to the suggested isotropy of the spatial power spectra [McDonald et al., 1974, 1975; Ierkic et al., 1977; Ferch and Sudan, 1977]. Figure 3 shows sample Fourier coefficients computed from spectra averaged over 2 sec near the beginning of the quasi-steady state of Model 2 and indicate an approximate power law in k for $1 \lesssim k/k_o \lesssim 14$. Similar results are found for Models 1 and 2.

Absolute Fourier coefficients a_n, b_n can then be defined using the best-fit spectral indices, p_n, q_n in the following manner:

$$I(\underset{\sim}{k},t) = a_o k^{-n} + \sum_n (a_n k^{-p_n} \cos n\theta + b_n k^{-q_n} \sin n\theta)$$

with the a_n, b_n found from least squares fitting. For time averaged spectra taken during the middle and end of the quasi-steady state of Model 2, Table 2 gives the best fit spectral indices and relative magnitudes (a_n/a_o, b_n/a_o) of the best fit coefficients that exceeded 0.1 and indicates that the power spectra are approximately isotropic. Similar results were obtained for the other two models. The best fit spectral indices were computed using a least squares fitting routine with errors equal to the standard deviations. The uncertainties in the relative coefficients reflect the statistical error in the mean of the time-averaged spectral estimates.

The computed power laws of the spatial power spectra $I(k) \sim k^{-n}$, $n = 3\text{-}4$, for λ:9-128 m are in agreement with previous rocket data ($n = 3 \pm 1$; λ:1-15 m, Prakash et al., 1969, 1970), recent numerical studies ($n \simeq 3.5$; λ:9-75 m, McDonald et al., 1974, 1975; $n = 3 \pm 1$; λ:9-128 m, Ferch and Sudan, 1977) and dimensional arguments ($n \gtrsim 3$, Ott and Farley, 1974). In addition the isotropic nature of the computed spatial power spectra for λ:9-128 m compares favorably with recent radar measurements of Type II irregularities at $\lambda = 3$ m [Ierkic et al., 1977].

It is of interest to study in more detail the isotropic part of the k-spectra. Figures 4a-4d illustrate the time evolution of the angle-averaged power spectra, viz., $I(k) = (2\pi)^{-1} \int_0^{2\pi} d\theta\, I(k,\theta)$ at $t = 0, 2, 13, 25$ sec for Model 2 ($V_d = 100$ m/sec). Initially, only one wavenumber $k = 1$ is excited (k is scaled in terms of the fundamental $k_o = 2/128\ m^{-1}$). The initial power residing in $k = 2$ to 14 is not physical but numerical in origin and results from discrete Fourier transformation. In the linear stages of the simulation, the power in the initially excited unstable mode increases. As the turbulence develops, the power in the linearly damped portion of the spectrum ($k > k_c \simeq 3$) also increases. Finally, nonlinear interactions in the fully developed turbulence has reduced the power in the initial wavenumber and brought the spectrum roughly in accordance with a power law.

In Fig. 5, for the quasi-steady states of Models 1-3, I(k) is plotted as a function of drift velocity V_d for several wavelengths. These curves indicate that the spectra follow an approximate power law in V_d, i.e., $I(k) \propto V_d^m$. Unfortunately, due to numerical instabilities

and computational cost, a larger range of drift velocities could not be studied. From radar backscatter observations at 3 m, a quadratic dependence of scattering cross section on drift velocity V_d has also been inferred [Balsley, 1969; Farley and Balsley, 1973].

TEMPORAL POWER SPECTRA

The temporal power spectra $I(k,\omega) \propto <|\delta n(k,\omega)|^2>$ were computed (see Appendix A) using the direct method [Blackman and Tukey, 1959]. Power spectral estimates from different time blocks were averaged to reduce the variance. The sampling frequency was chosen to be always greater than twice the frequencies in which there was measurable power in order to minimize aliasing. In many cases the spectra were further smoothed over adjacent channels using a Hann window. Final spectra at a particle (k_y,k_z), i.e., at a particular wavelength and angle to the electrojet drift, consisted of an average over 20.5 sec in the quasi-steady states of the three models. Several sample spectra were computed in order to estimate a sampling frequency which was taken to be 50 sec^{-1}. Both 128 and 256 point transforms were used. By choosing $n_y = k_y/k_o$, $n_z = k_z/k_o$ to lie between $0 \leq n_y \leq 14$ and $-14 \leq n_z \leq 14$, spectra are available from considerations of symmetry that cover the range $0° < \theta < 360°$ and $9 \text{ m} < \lambda < 128 \text{ m}$ where $\lambda = 2\pi/k$ and $\theta \tan^{-1}(k_y/k_z)$. Figures 6a-6c give sample computed spectra together with radar obtained spectra [Balsley and Farley, 1971] taken in the daytime equatorial electrojet for equivalent conditions. For $\lambda = 9$ m many of the computed spectra were of poor quality when integration times were less than 2 sec. All spectra were normalized to their maximum values. The principal characteristics of the spectra are their mean frequencies and average widths. We have analyzed for the three models the frequencies and widths of the computed spectra throughout the range of λ and θ.

MEAN SPECTRUM FREQUENCIES

The spectrum frequency, $\omega/2\pi$, is taken to be the average of the upper and lower half-power points. Extraneous peaks at zero frequency were disregarded. In Figures 7a-7c are displayed for Models 1-3 (V_d = 75, 100, 125 m/s) the computed spectrum frequencies as a function of k at the following fixed angles to the electrojet drift (also the principal radar angles): 90° (vertical), ± 45°, ± 30°. Also included at each angle are the frequencies of modes that propagate within 7.5° of these chosen angles. Positive angles refer to upward moving waves, negative angles to downward moving waves. Because some spectra were noisy all points could not be paired at the opposite angle. The linearly damped ($k > k_c$) and growing ($k < k_c$) modes are indicated along with the frequencies derived from the linear dispersion relation. The maximum error in each spectrum frequency is estimated to be 0.2 Hz. At the angles shown, the average spectrum frequencies computed from the quasi-steady turbulent state at the three drift velocities over the range of wavelengths 9-128 m are not, within error bounds, appreciably different from the linear results except at large k (short wavelengths). At these angles, aside from the vertical (90°), the computed spectrum frequencies are proportional to wavenumber, $\omega \alpha k$. Figure 8 illustrates for Model 2 (V_d = 100 m/s) the good agreement between the computed phase velocity, ω/k, in the steady turbulent state and the predicted dependence from linear theory, viz., $\omega/k = V_d(1 + \psi)^{-1} \cos\theta$. Similar fits are found for the other two models.

These results imply that even in the quasi-steady turbulent state with turbulent velocity fluctuations δV on the order of the mean drift V_d (see Fig. 1a-1c), the average frequencies can be found with the linear dispersion relation using the drift velocity V_d.

AVERAGE SPECTRUM WIDTHS

The average spectrum width, $\Delta\omega/2\pi$, is defined as the difference between the upper and lower half-power points. In Figures 9a-9c are displayed, for the three drift velocities, the mean spectral width as a function of k at the same angles. Linearly growing and damped wavelengths are also indicated and the linear damping rates shown. The maximum error in each computed spectrum width is estimated to be 0.4 Hz. At the angles shown, there is a definite trend for the average widths to increase with k, for all three drift velocities, a feature also noted in radar backscatter observations at 3 and 9 m [Balsley and Farley, 1971]. In addition, the widths at all angles and for all three drift velocities exceed the linear damping rates. Moreover, at fixed k, the width of the spectra of the linearly damped wavelengths increase with increasing drift velocity, a feature not predicted by linear theory. There seems to be no appreciable difference between the mean widths computed for the upward moving waves as compared to those of the downward moving waves except perhaps at large k. The exact dependence of $\Delta\omega$ on k, throughout the range of wavelengths studied, is not well-defined,

although, for example, the mean widths of the vertical modes (90°) for Model 2 fit well a power law in k, $\Delta\omega \sim k^n$ with $n \simeq 0.8$. Figure 10 shows $\Delta\omega/\omega$ at $\theta = 45°$ for Models 1-3. Over the range of k, $\Delta\omega/\omega$ exceeds 0.5 indicating strongly turbulent fluctuations. This is in rough agreement with radar observations [Balsley and Farley, 1971]. Similar plots are found for the other two models.

To examine the dependence of angle-averaged spectral width on wavenumber k for wavelengths not previously studied with radar, we have plotted in Figure 11 the numerically obtained angle-averaged frequency spread vs. k for the three drift velocities V_d = 75, 100, 125 m/sec. At all three drift velocities, the angle-averaged widths increase approximately monotonically with k. We have fitted these data, for each drift velocity, with a function of the form $(\gamma_k^2 + \Gamma_k^2)^{1/2}$ where γ_k is the linear growth rate and Γ_k is the predicted linewidth from Eq. (10). This function gives a reasonable fit after adjusting Γ_k by a constant of order unity. In this connection it would be useful to study the spectral characteristics of wavelengths greater than 9 m by radar.

The numerically obtained angle-averaged spectral width as a function of drift velocity V_d for several wavelengths is displayed in Figure 12. At theseewavelengths the data shows that the angle-averaged frequency spread is roughly proportional to V_d^m with $m \simeq 1.5$-2.5. From radar observations [Balsley, 1969; Farley and Falsley, 1973] it has been inferred that $I(k) \propto V_d^2$ giving for the angle-averaged spectral

broadening $\Gamma_k \propto V_d^2$. This agrees reasonably well with the curves shown in Figure 12. The experimentally observed linewidth $\Delta\omega$ from 9 m Type II radar backscatter observations [Balsley and Farley, 1971] is shown in Figure 13 as a function of drift velocity V_d. The dependence of $\Delta\omega$ with V_d appears linear as opposed to the quadratic results indicated by theory and the present numerical simulations. However, it must be noted that these results are obtained from one zenith angle and not angle-averaged. Furthermore, the effects on spectral width of the changing scattering volume is not well-defined throughout the range of drift velocities shown.

TEST WAVES

The magnitude of the power spectra of the short wavelength irregularities ($\lambda < 10$ m) is much smaller than the fundamental ($\lambda = 128$ m) by as much as four or five orders of magnitude. In order to study more closely the turbulent damping at the shorter wavelengths, test waves of the form $A \sin(k_y y + k_z z - \omega_k t)$ were launched in the quasi-steady states. The decay rates, τ_k^{-1}, of the test waves were found to be of the order of the spectral width $\Delta\omega$ of the power spectra computed at the wavelength of the test waves. The wavelength λ and the propagation angle θ of the test waves were taken to be 9, 10 m and $\pm$ 45°, respectively, with the amplitude A fixed at 0.04. This amplitude corresponds to the approximate quasi-steady state amplitude of the turbulent density fluctuations. Figure 14 gives an example of the decay of a sample 10 m test wave launched in the quasi-steady state of Model 2. Table 3 compares the nonlinear damping as computed from the spectral width, test wave decay rates, and the theoretical prediction for wavelengths studied in Models 1-3. The agreement between spectral width and test wave decay rates is reasonable. Better agreement cannot be expected since the spectra were computed by averaging many samples whereas the test wave decay rates are found using only one sample. However, the trend of increasing spectral width with decreasing wavelength is also noted in the decay rates of the large amplitude short wavelength test waves.

CONCLUSION

We have computed the temporal and spatial power spectra from numerical simulation of Type II irregularities in the daytime equatorial electrojet. The overall level of turbulent density fluctuation appears to increase with the electrojet drift velocity, V_d, in the range 75-125 m/s. Appreciable excitation of vertical and oblique waves is seen at drift velocities of 75 and 125 m/s. This supplements similar results of Ferch and Sudan (1977) at V_d = 100 m/s and provides further support for the two-dimensional model of Sudan et al. (1973).

At the three drift velocities studied (75, 100, 125 m/s) and in the wavelength range of approximately 9-128 m the computed time-averaged spatial power spectra I(k) are, on the average, found to be isotropic and follow a power law in k($I(k) \propto k^{-n}$, $n = 3.5 \pm 0.5$). This is in agreement with experimental results [Prakash et al., 1969, 1971, 1972; Ierkic et al., 1977 for λ = 9 m], numerical simulations [McDonald et al., 1974, 1975; Ferch and Sudan, 1977] and dimensional arguments [Ott and Farley, 1974]. In addition, some evidence is found which suggests that $I_k \propto V_d^m$, in agreement with Type II radar observations [Balsley, 1969; Farley and Balsley, 1973].

The numerically computed temporal power spectra compare favorably with several 9 m Type II radar spectra taken in the daytime equatorial electrojet [Balsley and Farley, 1971]. The numerical spectra are computed with known electrojet parameters with the radar spectra

being integrated over a small region of the electrojet due to limited resolution (1-3 km). In addition, only a limited number of interacting modes can be kept in the simulation due to finite grid size and computer storage limitations and spectral integration times must be minimized. These factors make direct comparison between numerical and radar spectra difficult to assess.

In the turbulent quasi-steady states of the three models studied, the mean spectrum frequencies of the numerically obtained spectra agree well, within error bounds, with linear theory, except at short wavelengths. The average spectrum widths, on the other hand, in the wavelength range 9-128 m are greater than the linear damping rates and increase with decreasing wavelength. Also, at a fixed wavelength, the average widths of the linearly damped modes increase with drift velocity in the range 15-125 m/s, a feature not predicted by the linear theory of the gradient-drift instability. No appreciable difference is seen in the spectral widths of the upward moving waves as compared with the downward moving waves. Moreover the width to mean ratios of the computed spectra suggest strongly turbulent fluctuations in agreement with radar observations [Balsley and Farley, 1971].

There remains some noise-like features in the computed spectral characteristics of the short wavelength ($\lambda < 10$ m) irregularities. This is to be expected due to resolution limitations. In the models studied a grid mesh of 64 x 64 points is used which allows Fourier components of up to wavenumber 32 in each direction. Components with wavenumbers greater than 16, therefore, are subject to possibly serious

distortion from aliasing errors. The highest wavenumber studied in Model 1-3 was 14 (9.1 m). The overall trend of increasing linewidth with decreasing wavelength is noted in the decay rates of the large amplitude short wavelength test waves. The effects on the spectra at the short wavelengths due to other sources of error, e.g., spatial and temporal truncation errors, could not be fully investigated due to the high computational cost of the spectral integration times. However, in Model 3, after restarting near the quasi-steady state, several short wavelength spectra were computed after halving the time step thereby reducing the time truncation error. No appreciable differences were found in spectral features.

Finally, the power law ($I_k \propto k^{-n}$, n = 3-4) of the turbulence and the scaling of the frequency broadening Γ_k with wavenumber k and drift velocity V_d lend support to the strong turbulence theory of Sudan and Keskinen (1977) which predicts $\Gamma_k \propto V_d\, k^2\, I_k^{1/2}$ with $I_k \propto k^{-n}$, $n \simeq 3.2$.

ACKNOWLEDGMENTS

We thank D. T. Farley, B. Fejer, and M. Ierkic for valuable discussions and B. Balsley for providing unpublished data. All computations were carried out on the CDC 7600 located at the National Center for Atmospheric Research, Boulder, Colorado. Acknowledgment is made to NCAR, which is sponsored by the NSF, for this computing time. This work was supported in part by NSF Grant #GA-35530X and in part by ONR Contract #N00014-67-A-0077-0031.

APPENDIX A:

METHOD OF COMPUTING TEMPORAL POWER SPECTRA

Fourier expanding $\delta n(x,t)$ over a square of edge L in the time interval T

$$\delta n(x,t) = \sum_{k,\omega} \delta n(\underset{\sim}{k},\omega) \exp\{i(\underset{\sim}{k}\cdot\underset{\sim}{x} - \omega t)\} \tag{A.1}$$

$$\delta n(\underset{\sim}{k},\omega) = (2\pi)^{-3}(L^2T)^{-1} \int d^2x\, dt\, \delta n(\underset{\sim}{x},t) \exp\{-i(\underset{\sim}{k}\cdot\underset{\sim}{x} - \omega t)\} \tag{A.2}$$

where $\underset{\sim}{x} = (y,z)$, $\underset{\sim}{k} = (k_y,k_z)$ and defining the normalized temporal power spectrum $I_{\underset{\sim}{k},\omega}$

$$\left\langle \left|\frac{\delta n}{no}\right|^2 \right\rangle = \int d^2k\, d\omega\, I_{\underset{\sim}{k},\omega} \tag{A.3}$$

we find for homogeneous and stationary turbulence

$$I_{\underset{\sim}{k},\omega} = \lim_{L,T\to\infty} \frac{L^2T}{(2\pi)^3} \left\langle \left|\frac{\delta n(\underset{\sim}{k},\omega)}{n_o}\right|^2 \right\rangle \tag{A.4}$$

where the angle brackets denote an ensemble average, viz., the average over a large number of identical systems of which the system under study is a member. In the quasi-steady state, the ensemble average is equivalent to a time average over any one system of the ensemble. This direct method of computing the temporal power spectra is more desirable than the method of autocorrelations due to computer storage

limitation and the relative speed of the fast Fourier transform (FFT). Both methods can be shown to be equivalent [Blackman and Tukey, 1959].

In order to compute $I_{\underset{\sim}{k},\omega}$ in practice we must first compute $\delta n(\underset{\sim}{k},\omega)$ which in discrete form can be written for fixed $\underset{\sim}{k}$

$$\delta n(\underset{\sim}{k},\ell\Delta f) = \frac{1}{N}\sum_{j=0}^{N-1} \delta n(\underset{\sim}{k},j\Delta t)\exp\{-2\pi ij\ell/N\} \qquad (A.5)$$

where N is the number of time samples, $\ell = 0, 1, \ldots, N-1$, $j = 0, 1, \ldots, N-1$, $\Delta f = T$, T the total integration time, Δt is the sampling period. Power spectral estimates from successive time blocks were averaged to reduce the variance. The sampling frequency $(\Delta t)^{-1}$ was chosen to be always greater than twice the frequencies in which there was measurable power in order to minimize chasing. This was accomplished by first computing the highest frequencies in the system. In our case, these were found at the shortest wavelengths ($14 \lesssim k/k_o \gtrsim 10$, $9\text{ m} \lesssim \lambda \lesssim 12\text{ m}$). In Models 1-3, the maximum frequencies corresponding to these short wavelengths was found, by trial and error, to be less than 10 sec^{-1}.

REFERENCES

Balsley, B. B., Some characteristics of non-two-stream irregularities in the equatorial electrojet, J. Geophys. Res. 74, 2333-2347, 1969.

Balsley, B. B., and D. T. Farley, Radar studies of the equatorial electrojet at three frequencies, J. Geophys. Res. 76, 8341-8351, 1971.

Balsley, B. B., and D. T. Farley, Radar observations of two-dimensional turbulence in the equatorial electrojet, J. Geophys. Res. 78, 7471-7479, 1973.

Blackman, R. B., and J. W. Tukey, The measurement of power spectra, Dover, New York, 1959.

Dupree, T. H., A perturbation theory for strong plasma turbulence, Phys. Fluids 9, 1773-1782, 1966.

Farley, D. T., and B. B. Balsley, Instabilities in the equatorial electrojet, J. Geophys. Res. 78, 227-239, 1973.

Fejer, B. G., D. T. Farley, B. B. Balsley, and R. F. Woodman, Vertical structure of the VHF backscattering region in the equatorial electrojet and the gradient drift instability, J. Geophys. Res. 80, 1313-1324, 1975.

Fejer, B. G., D. T. Farley, B. B. Balsley, and R. F. Woodman, Radar observations of two-dimensional turbulence in the equatorial electrojet, 2, J. Geophys. Res. 81, 130-134, 1976.

Ferch, R. L., and R. N. Sudan, Numerical simulations of type II gradient drift irregularities in the equatorial electrojet, J. Geophys. Res. 82, 2283-2288, 1977.

Ierkic, M., B. G. Fejer, and D. T. Farley, Angular dependence of the scattering cross section of equatorial electrojet irregularities, Trans., A.G.U. 58, 449, 1977.

Kadomtsev, B. B., Plasma Turbulence (Academic, New York, 1965), Chap. III.

Keskinen, M., R. L. Ferch, and R. N. Sudan, Power spectrum studies of numerical simulation of ionospheric gradient-drift turbulence, Trans., A.G.U. 58, 521, 1977.

Knox, F. B., A contribution to the theory of the production of field-aligned ionization irregularities in the equatorial electrojet, J. Atmos. Terr. Phys. 26, 239-249, 1964.

Kraichnan, R. H., The structure of isotropic turbulence at very high Reynolds numbers, J. Fluid Mech. 5, 497, 1959.

Maeda, K., T. Tsuda, and H. Maeda, Theoretical interpretation of the equatorial sporadic E layers, Rep. Ionos. Space Res. Jap. 17, 3, 1963.

McDonald, B. E., T. P. Coffey, S. L. Ossakow, and R. N. Sudan, Preliminary report of numerical simulation of type 2 irregularities in the equatorial electrojet, J. Geophys. Res. 79, 2551-2554, 1974.

McDonald, B. E., T. P. Coffey, S. L. Ossakow, and R. N. Sudan, Numerical studies of type 2 equatorial electrojet irregularity development, Radio Sci. 10, 247-254, 1975.

Orszag, S. A., Analytical theories of turbulence, J. Fluid Mech. 41, 363-386, 1970.

Ott, E., and D. T. Farley, The K spectrum of ionospheric irregularities, J. Geophys. Res. 79, 2469-2472, 1974.

Prakash, S., S. P. Gupta, and B. H. Subbaraya, Irregularities in the equatorial E region over Thumba, Radio Sci. 4, 791-796, 1969.

Prakash, S., S. P. Gupta, and B. H. Subbaraya, Nighttime equatorial E region irregularities, Planet Space Sci. 18, 1307-1318, 1970.

Prakash, S., B. H. Subbaraya, and S. P. Gupta, Rocket measurements of ionization irregularities in the equatorial ionosphere at Thumba and identification of plasma irregularities, Indian J. Radio Space Phys. 1, 72-80, 1972.

Reid, G. C., The formation of small-scale irregularities in the ionosphere, J. Geophys. Res. 73, 1627-1640, 1968.

Rogister, A., and N. D'Angelo, Type II irregularities in the equatorial electrojet, J. Geophys. Res. 75, 3879-3887, 1970.

Rogister, A., Nonlinear theory of cross-field instability with application to the equatorial electrojet, J. Geophys. Res. 77, 2975-2981, 1972.

Rognlien, T. D., and J. Weinstock, Nonlinear saturation of the gradient drift instability in the equatorial electrojet, J. Geophys. Res. 78, 6808-6810, 1973.

Rognlien, T. D., and J. Weinstock, Theory of the nonlinear spectrum of the gradient drift instability in the equatorial electrojet, J. Geophys. Res. 79, 4733-4746, 1974.

Sato, T., Nonlinear theory of the cross-field instability-explosive mode coupling, Phys. Fluids 14, 2426-2435, 1971.

Sato, T., Unified theory of type I and II irregularities in the equatorial electrojet, J. Geophys. Res. 78, 2232-2243, 1973.

Sato, T., and T. Tsuda, Computer study on non-linear cross-field instability, Phys. Fluids 10, 1262, 1967.

Sato, T., and T. Ogawa, Self-consistent studies of two-dimensional large-scale ($\sim$ 100 m) electrojet irregularities, J. Geophys. Res. 81, 3248-3256, 1976.

Sleeper, A. M., and J. Weinstock, Nonlinear theory of density fluctuations in turbulent plasmas, Phys. Fluids 15, 1507-1514, 1972.

Sudan, R. N., J. Akinrimisi, and D. T. Farley, Generation of small-scale irregularities in the equatorial electrojet, J. Geophys. Res. 78, 240-248, 1973.

Sudan, R. N., and M. Keskinen, Theory of strongly turbulent two-dimensional convection of low-pressure plasma, Phys. Rev. Lett. 38, 966, 1977.

Weinstock, J., Formulation of a statistical theory of strong plasma turbulence, Phys. Fluids 12, 1045-1058, 1969.

Weinstock, J., and R. H. Williams, Nonlinear theory of macro-instabilities and enhanced transport in plasmas, Phys. Fluids 14, 1472-1480, 1971.

Weinstock, J., and A. M. Sleeper, Nonlinear saturation of type I irregularities in the equatorial electrojet, J. Geophys. Res. 77, 3621-3624, 1972.

Whitehead, J. D., The equatorial electrojet and the gradient instability, J. Geophys. Res. 76, 3116-3126, 1971.

TABLE 1

SUMMARY OF MODEL PARAMETERS

Model	Mesh Points	Size, m	Initial Amplitude of Perturbation, % Horizontal	Vertical	V_d, m/s	L,m
1	64 x 64	128	3	1	75	6000
2	64 x 64	128	3	1	100	6000
3	64 x 64	128	3	1	125	6000

TABLE 2

BEST FIT POWER LAWS AND RELATIVE COEFFICIENTS FOR MODEL 2

Time(sec)	Timestep	n	a_2/a_o	P_2	a_8/a_o	P_8	b_4/a_o	q_4
28 - 30	14000 - 15000	3.3 ± .5	0.2 ± .03	3.4 ± .6	0.1 ± .02	3.6 ± .6	0.2 ± .02	3.7 ± .6

		n	a_2/a_o	P_2	a_4/a_o	P_4	b_2/a_o	q_2
36 - 38	18000 - 19000	3.6 ± .4	0.3 ± .04	3.9 ± .7	0.1 ± .02	4.2 ± .5	0.1 ± .03	4.0 ± .6

TABLE 3

Comparison of nonlinear damping as derived from spectral width, test wave decay rates, and theory for Model 2. Γ_{SW} ($= \Delta\omega/(8 \ln 2)^{1/2}$) is nonlinear frequency broadening from full width at half maximum, $\Delta\omega$, of computed spectra taken at 45° to electrojet drift and assumed Gaussian. Γ_{TW} ($= \tau^{-1}/2$) is broadening from decay of test waves launched at 45° and taken to be of form $\exp(-t/\tau)$. Γ_k is nonlinear broadening as computed from theory with $\alpha = 1/3$.

λ,m	$\Gamma_{SW}(sec^{-1})$	$\Gamma_{TW}(sec^{-1})$	$\Gamma_k(sec^{-1})$
9	1.8	4.4	1.1
10	1.7	1.5	0.9

FIGURE CAPTIONS

Figure 1. Maximum total density fluctuation $\delta n/n$, amplitude of initially growing mode $A_{1,0}$, and maximum horizontal and vertical turbulent velocities V_n and V_v as function of time in seconds.

(a) Model 1.

(b) Model 2.

(c) Model 3.

Figure 2. Contour plots of density fluctuation δn for Model 3 (V_d = 125 $msec^{-1}$). Contour lines represent equal increments in δn between maximum (+ signs) and minimum (- signs). Horizontal axis is y(direction of electron drift) and vertical axis is z(vertical). Scale for $A_{1,0}$ reads one half of $\delta n/n$ scale.

(a) t = 0, $\delta n/n$ = .04, $A_{1,0}$ = 6.14, $V_{H,max}$ = 100.

(b) t = 2, $\delta n/n$ = .06, $A_{1,0}$ = 9.22, $V_{H,max}$ = 173.

(c) t = 4, $\delta n/n$ = .14, $A_{1,0}$ = 13.61, $V_{H,max}$ = 427.

(d) t = 12, $\delta n/n$ = .07, $A_{1,0}$ = 5.81, $V_{H,max}$ = 251.

(e) t = 26, $\delta n/n$ = .068, $A_{1,0}$ = 4.83, $V_{H,max}$ = 212.

(f) t = 34, $\delta n/n$ = .06, $A_{1,0}$ = 4.53, $V_{H,max}$ = 192.

Figure 3. Sample time averaged Fourier coefficients I(k) denoted by closed circles, and $f_2(k)$ denoted by open circles, computed near beginning of quasi-steady states of Model 2.

Figure 4. Time evolution of I(k) vs. k for Model 2 (V_d = 100 $msec^{-1}$).

(a) t = 0 sec.

(b) t = 2 sec.

(c) t = 13 sec.

(d) t = 25 sec.

Figure 5. Plot of I(k) vs. V_d for several wavelengths λ in the quasi-steady states of Models 1-3.

Figure 6. Comparison between computed and radar-obtained power spectra $I_{k,\omega}$ vs. frequency in Hz. Solid curve from numerical simulation; dotted curve from radar backscatter observations at 16.25 MHz (λ = 9.2 m) [Balsley and Farley, 1971]; $\Delta\omega/2\pi$ is the difference of the frequencies at the upper and lower half-power points.

(a) Radar spectrum received from 60° east of vertical; simulation spectrum taken at $\tan^{-1}(k_y/k_z) = -30.2°$.

(b) Radar spectrum received from 45° west of vertical; simulation spectrum taken at $\tan^{-1}(k_y/k_z) = 45°$.

(c) Simulation spectrum taken at $\tan^{-1}(k_y/k_z) = 90°$ and $2\pi/(k_y^2 + k_z^2)^{1/2}$ = 16 m. Vertical 9 m spectra have not been studied with radar due to critical frequency limitations.

Figure 7. Computed spectrum frequencies as functions of k for Models 1-3. The spectrum frequency $\omega/2\pi$ (Hz) is the average of the frequencies at the upper and lower half-power points. Solid-dashed line is frequency from linear theory at V_d = 125 $msec^{-1}$; solid line for V_d = 100 $msec^{-1}$; dashed line for V_d = 75 $msec^{-1}$. Arrow marks critical wavenumber k_c from linear theory.

(a) $\theta = \tan^{-1}(k_y/k_z) = 90°$; linear theory predicts nonpropagating vertical modes.

(b) $\theta = 45°, -45°$.

(c) $\theta = 30°, -30°$.

Figure 8. Comparison of computed phase velocity, ω/k, in steady state with predicted dependence from linear theory ($\omega/k \propto \cos\theta$) for Model 2 ($V_d$ = 100 $msec^{-1}$). Solid line is linear theory at V_d = 100 $msec^{-1}$.

Figure 9. Computed spectrum line width as functions of k for Models 1-3. Solid line is linear damping rate. Arrow marks critical wavenumber k_c from linear theory.

(a) $\theta = 90°$.

(b) $\theta = 45°, -45°$.

(c) $\theta = 30°, -30°$.

Figure 10. Plot of $\Delta\omega/\omega$ for Models 1-3 at $\theta = 45°$.

Figure 11. Comparison between numerically obtained angle-averaged spectral widths and predicted angle-averaged nonlinear frequency broadening Γ_k vs. k for Models 1-3. Dots, circles, and triangles show $\Delta\omega$ from simulation averaged over angles; dotted curve gives γ_k from linear theory; solid lines show $(\Gamma_k^2 + \gamma_k^2)^{1/2}$; at large k, γ_k is comparable to Γ_k in simulations; numerical factors are adjusted for best fit.

Figure 12. Plot of computed angle averaged spectral linewidth $\Delta\omega$ vs. V_d at several different wavelengths; numerical factors are adjusted for best fit.

Figure 13. Plot of $\Delta\omega$ vs. electrojet drift velocity V_d from radar observations at 45° [Balsley and Farley, 1973] for $\lambda = 9$ m.

Figure 14. Plot of decay of squared amplitude of 10 m test wave vs. time in seconds launched in Model 2. Decay time z is taken to be time at which amplitude falls to e^{-1} of initial amplitude.

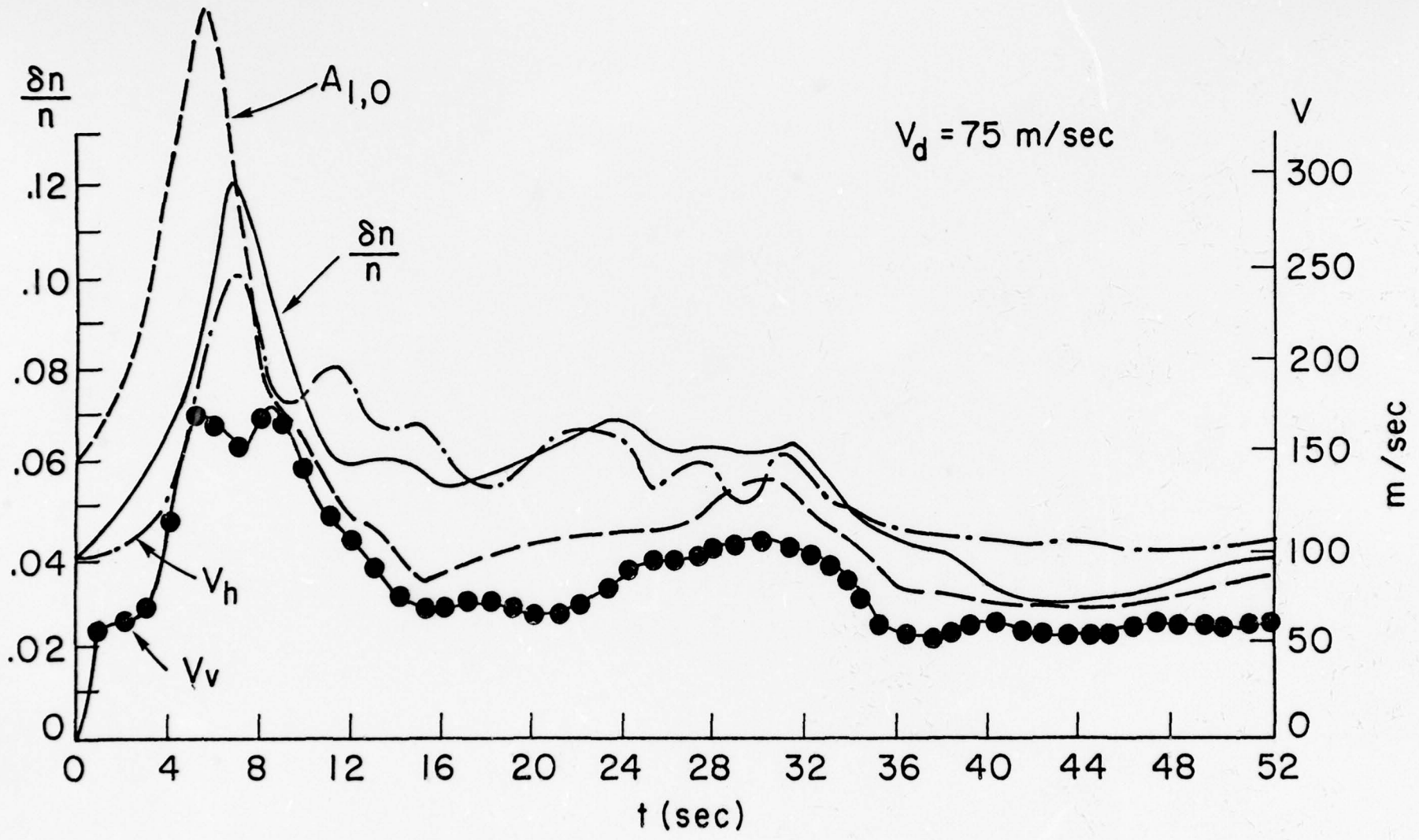
δn/n
A1,0
δn/n
Vd = 75 m/sec
V
300
250
200
150
100
50
0
m/sec
.12
.10
.08
.06
.04
.02
0
Vh
Vv
0
4
8
12
16
20
24
28
32
36
40
44
48
52
t (sec)

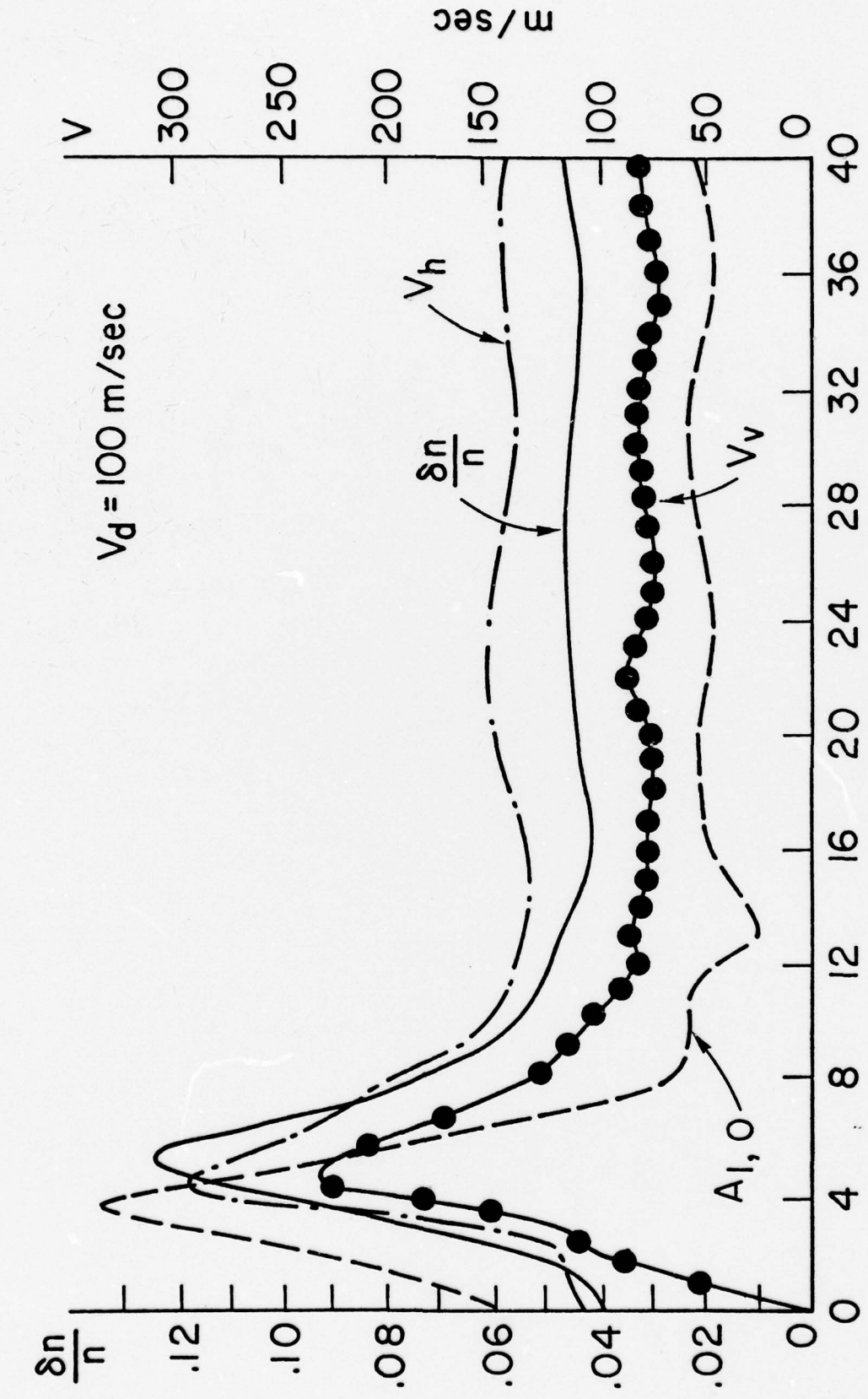
V
300
250
200
150
100
50
0
m/sec
V_d = 100 m/sec
V_h
$\frac{\delta n}{n}$
V_v
$A_{1,0}$
$\frac{\delta n}{n}$
.12
.10
.08
.06
.04
.02
0
0
4
8
12
16
20
24
28
32
36
40
t (sec)

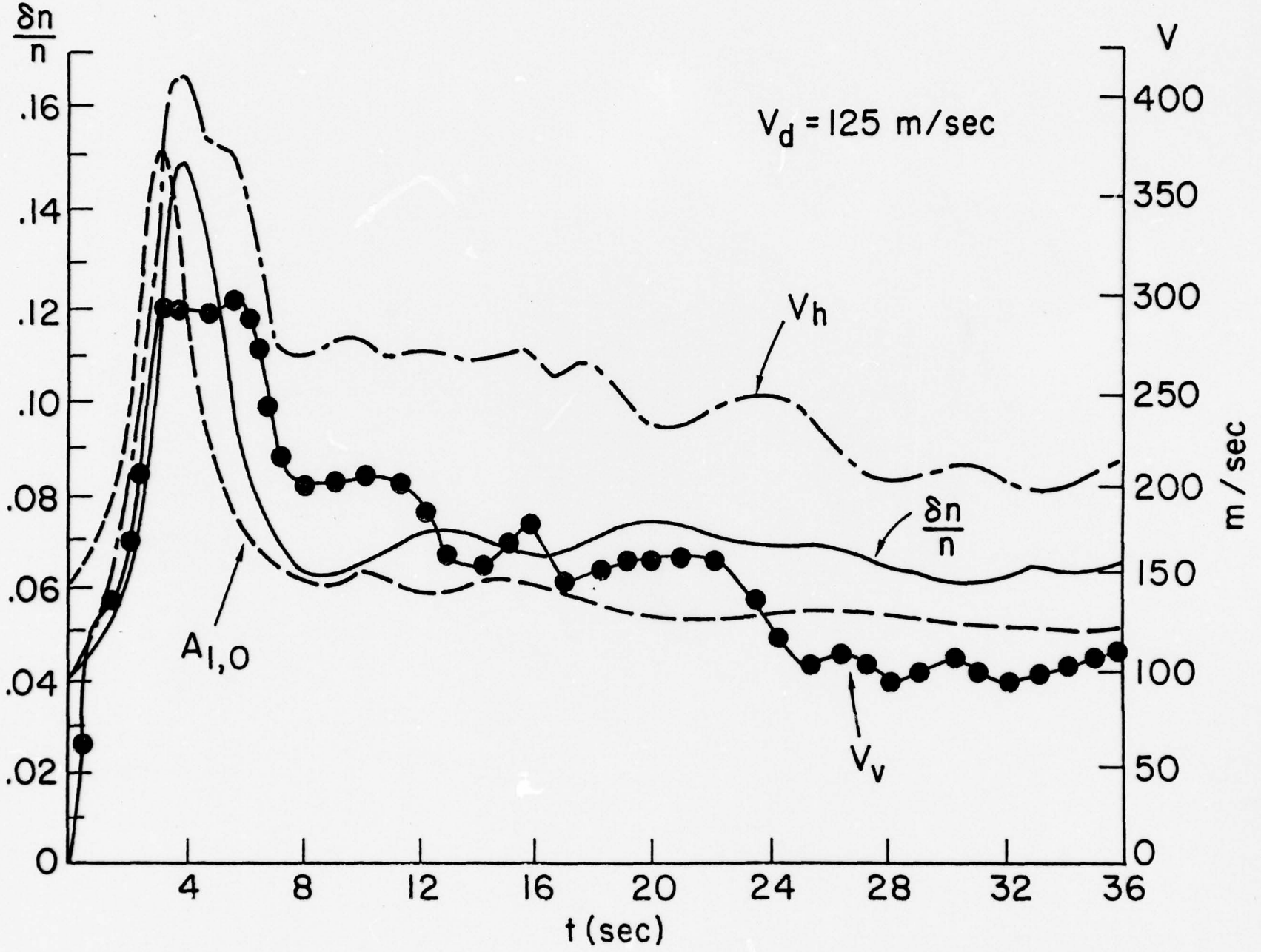
δn/n
V
.16
.14
.12
.10
.08
.06
.04
.02
0
400
350
300
250
200
150
100
50
0
4
8
12
16
20
24
28
32
36
t (sec)
m/sec
V_d = 125 m/sec
V_h
$\frac{\delta n}{n}$
$A_{1,0}$
V_v

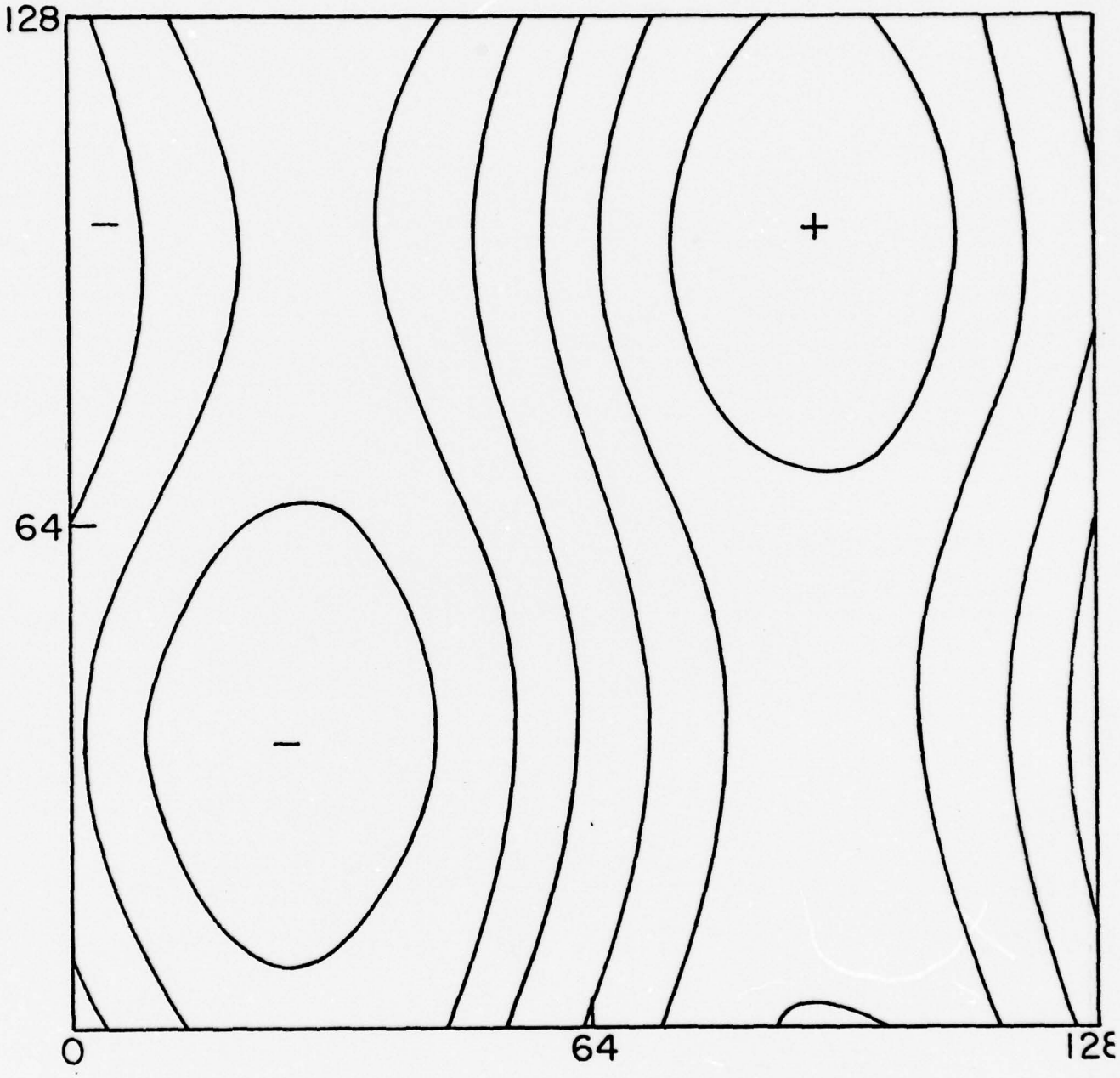
128
64
0
64
128
−
+
−

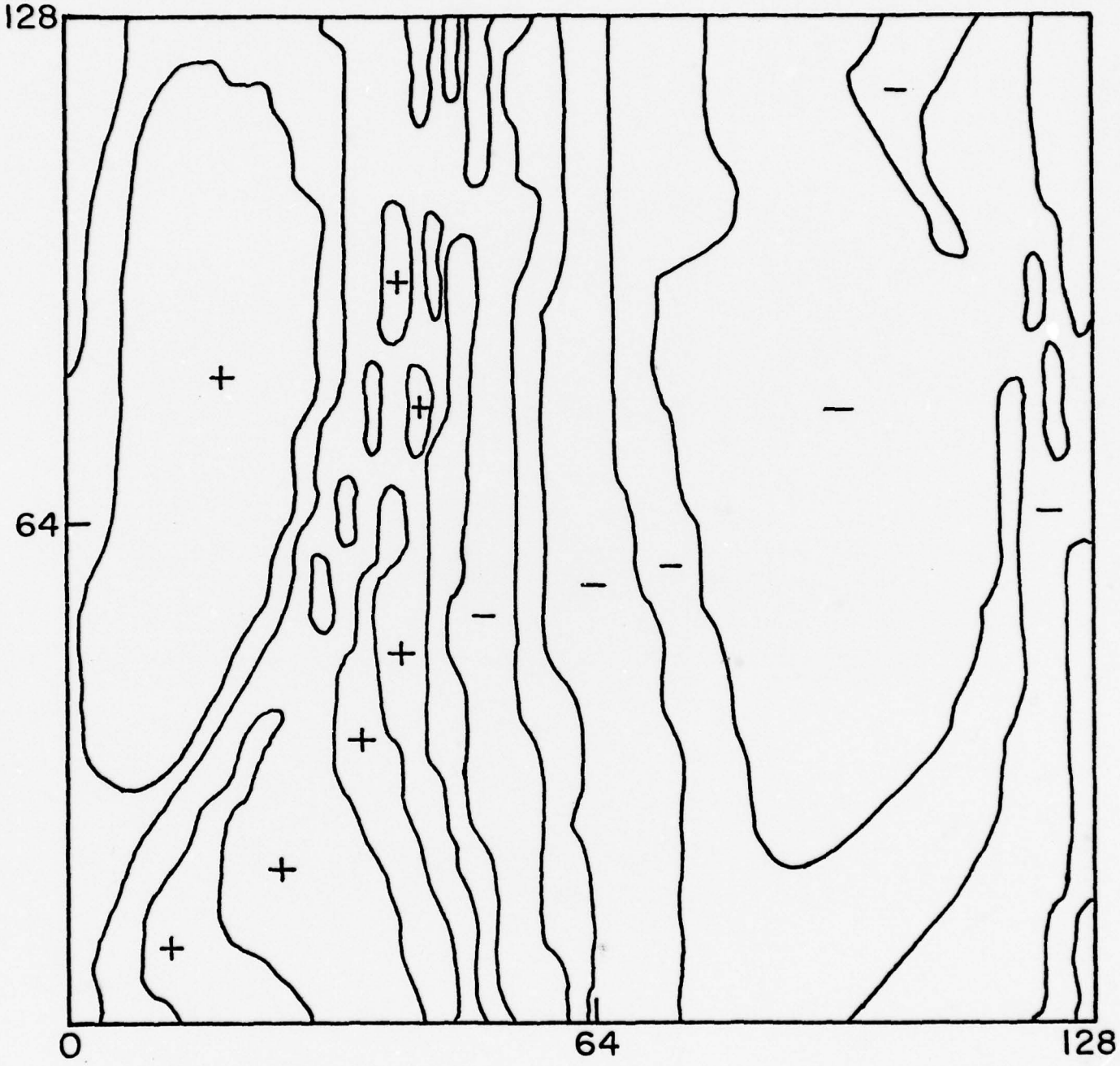
128
64
0
64
128
+
+
+
+
+
+
+
−
−
−
−
−
−

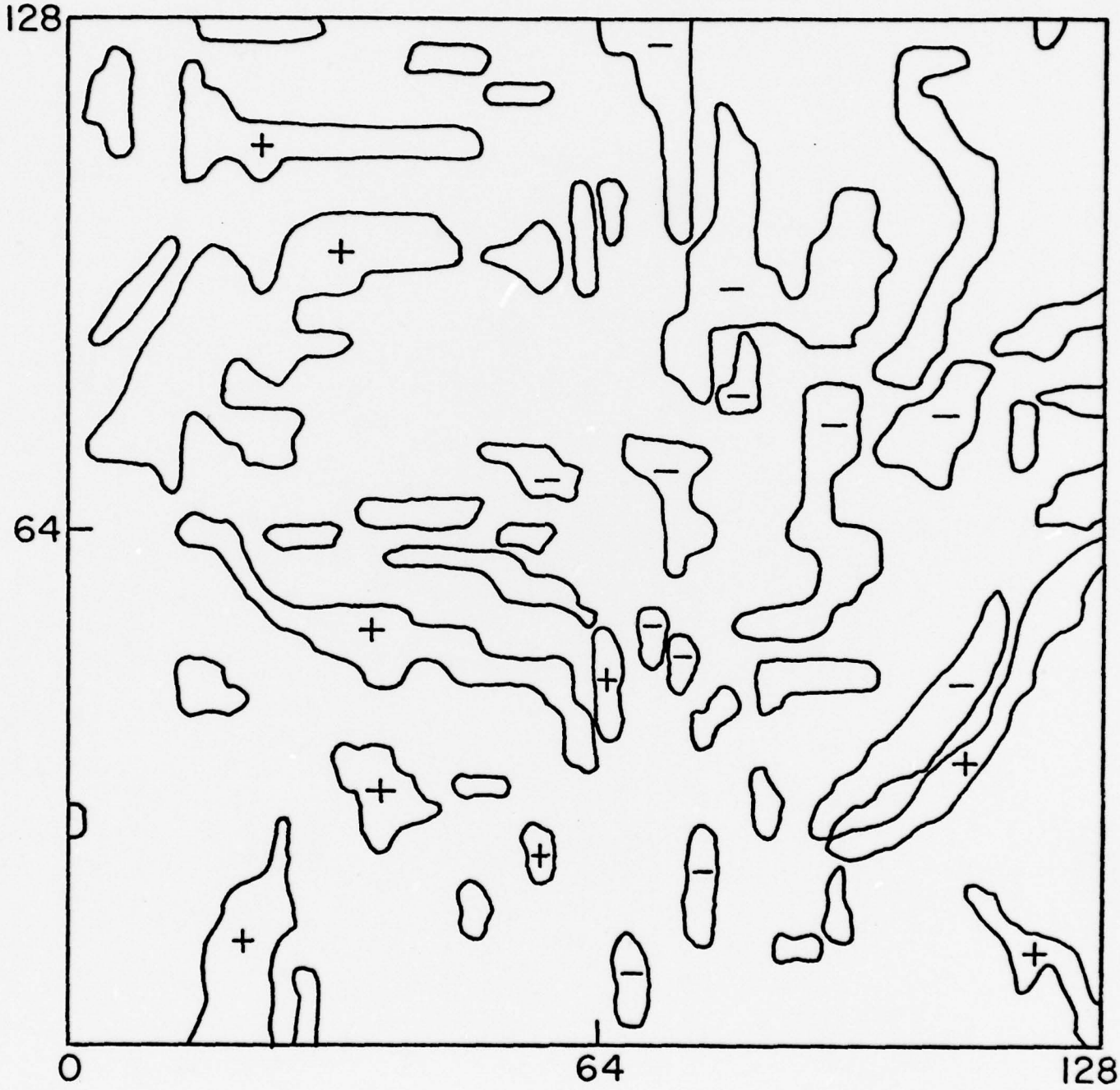
128
64
0
64
128

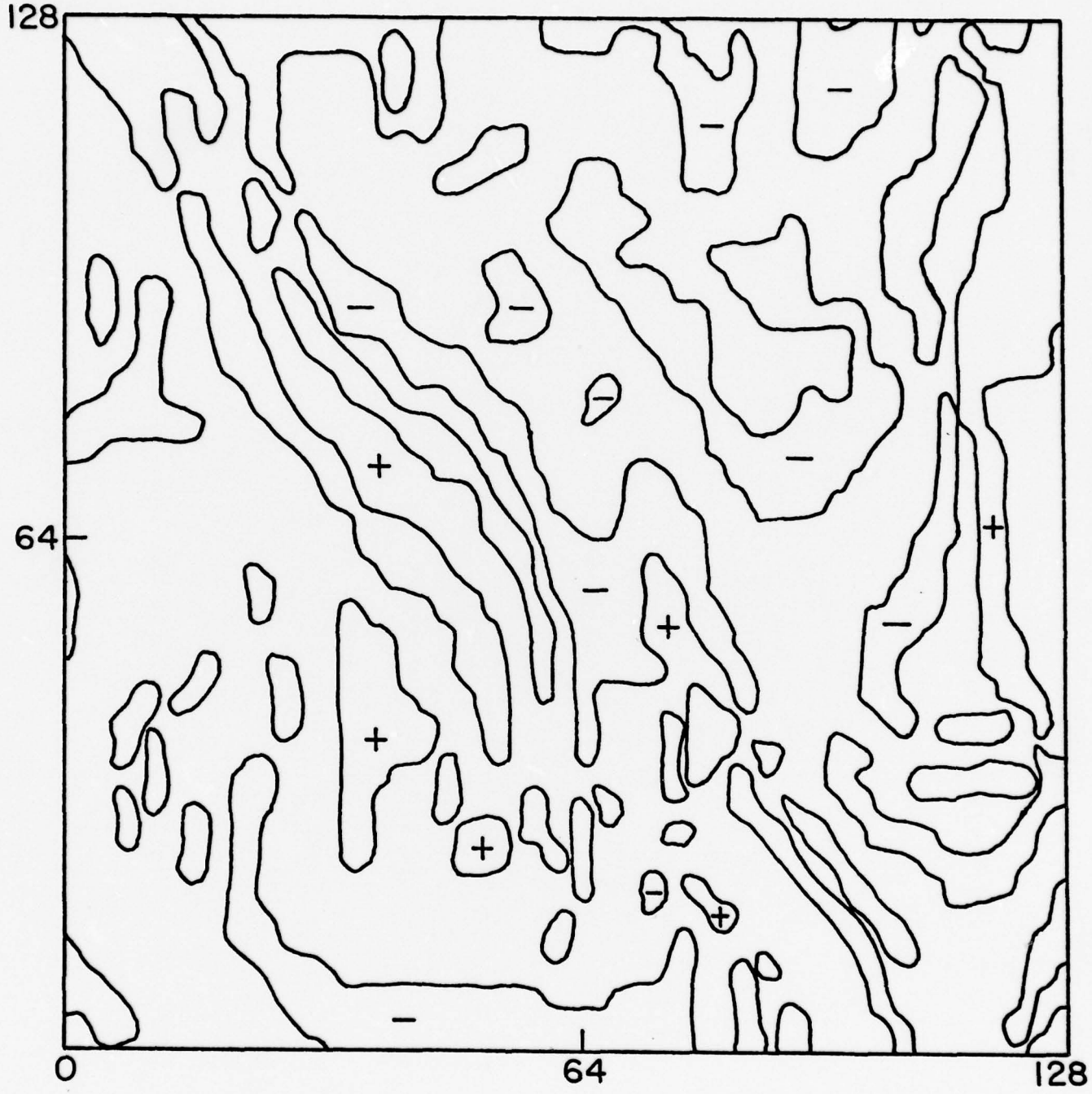
128
64
0
64
128

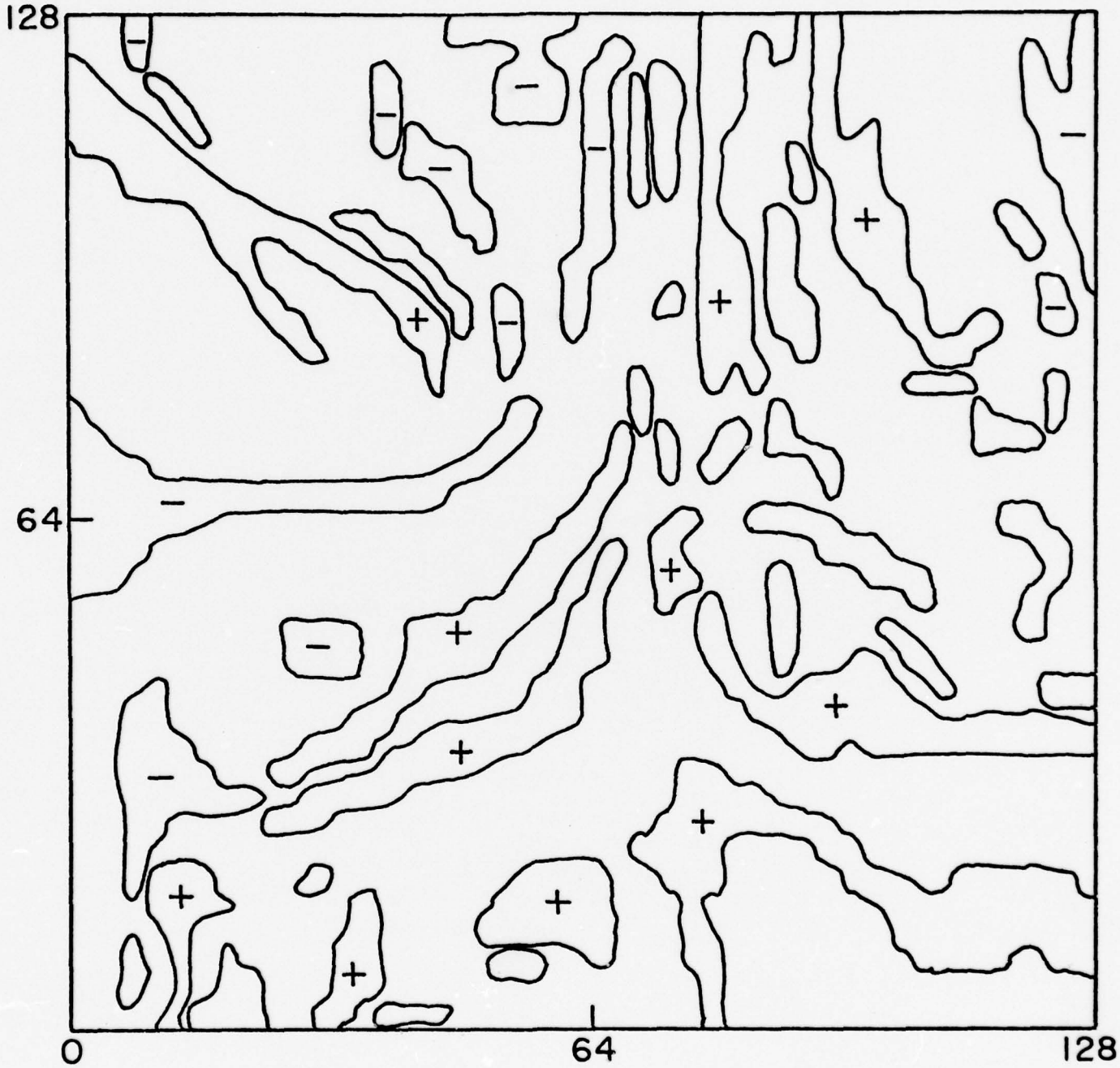
128
64
0
64
128

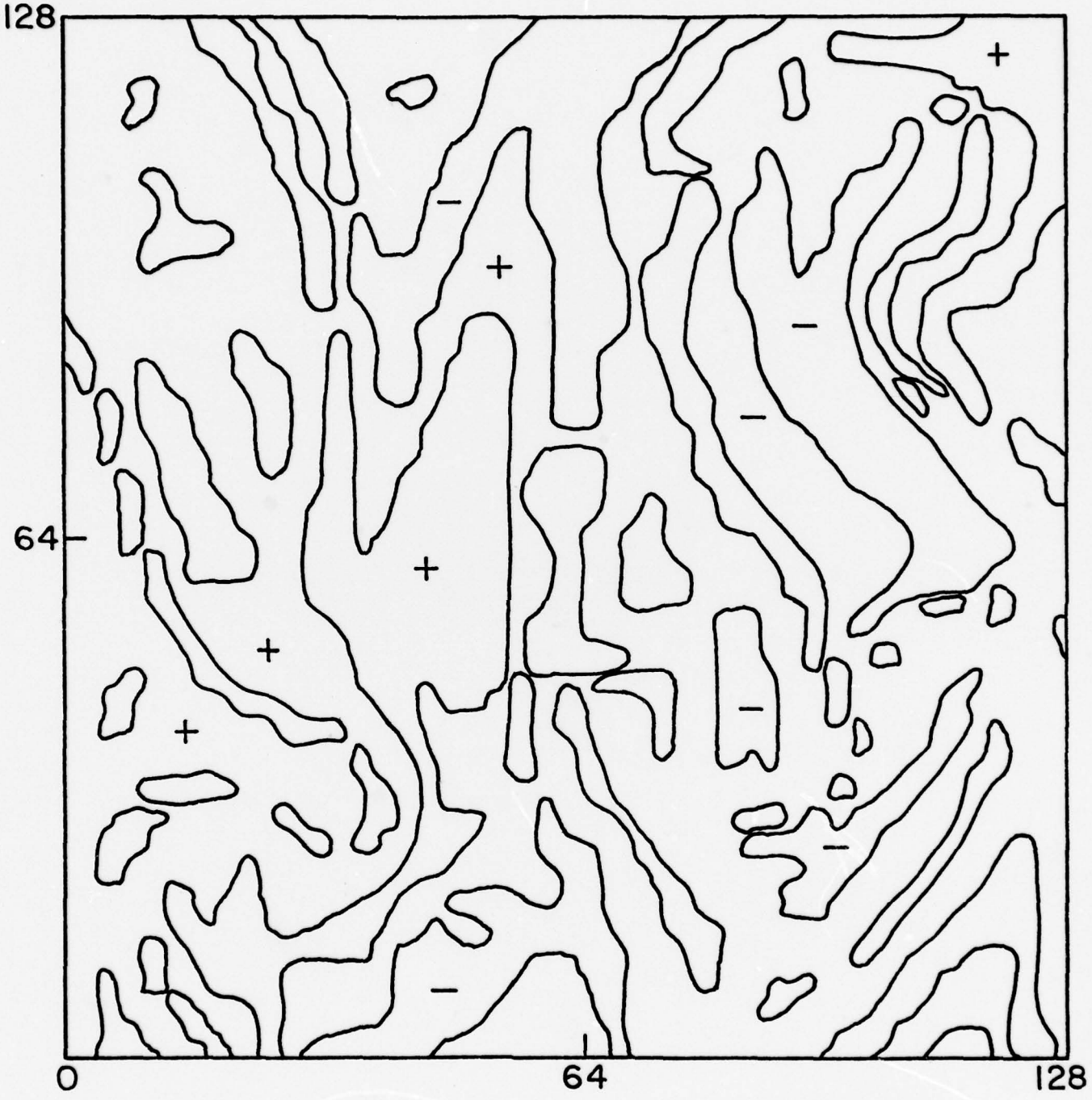
128
64
0
64
128
+
−
+
−
−
+
+
+
−
−
−

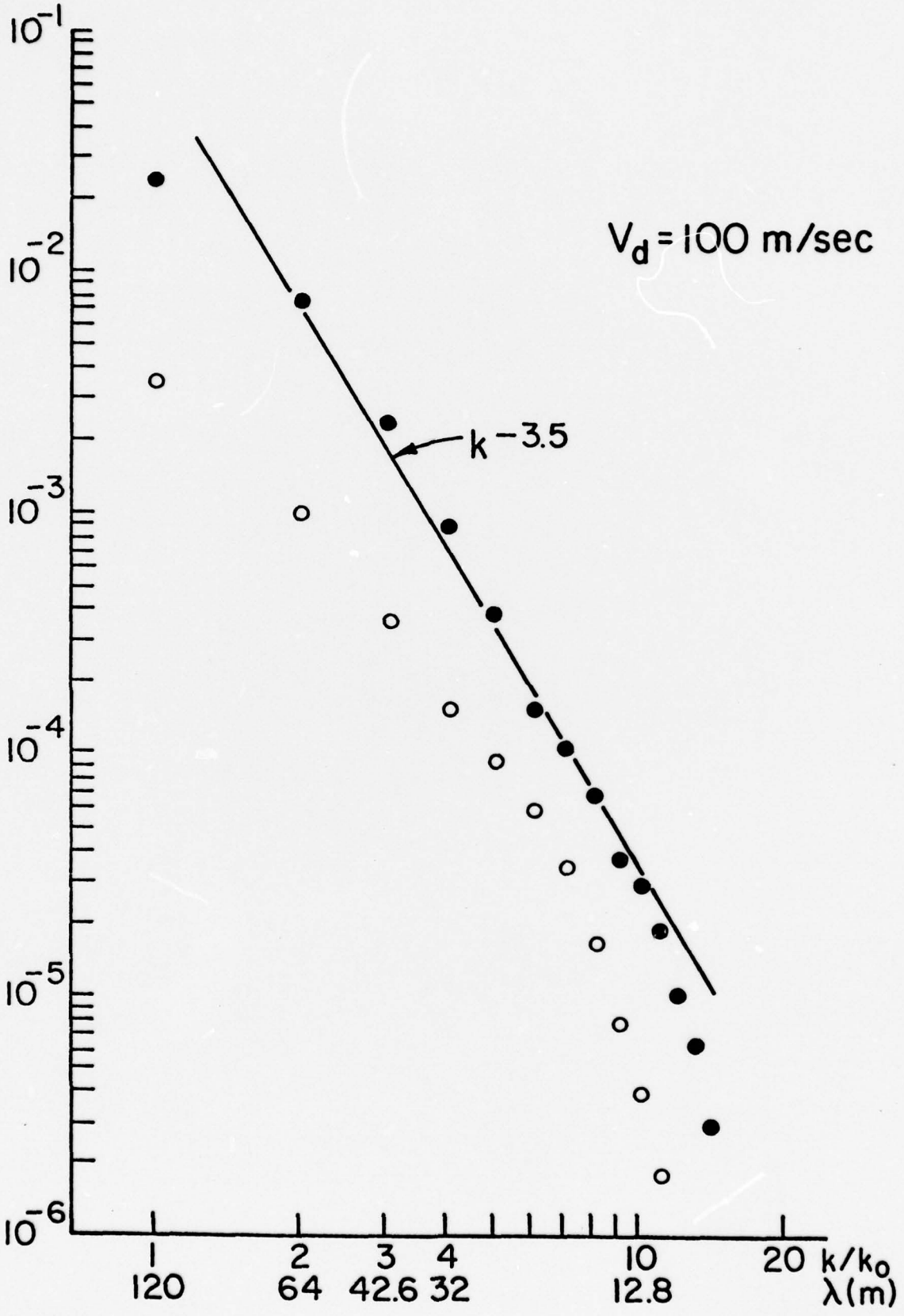
10^{-1}
10^{-2}
10^{-3}
10^{-4}
10^{-5}
10^{-6}
$V_d = 100$ m/sec
$k^{-3.5}$
1
2
3
4
10
20
k/k_o
120
64
42.6
32
12.8
λ(m)

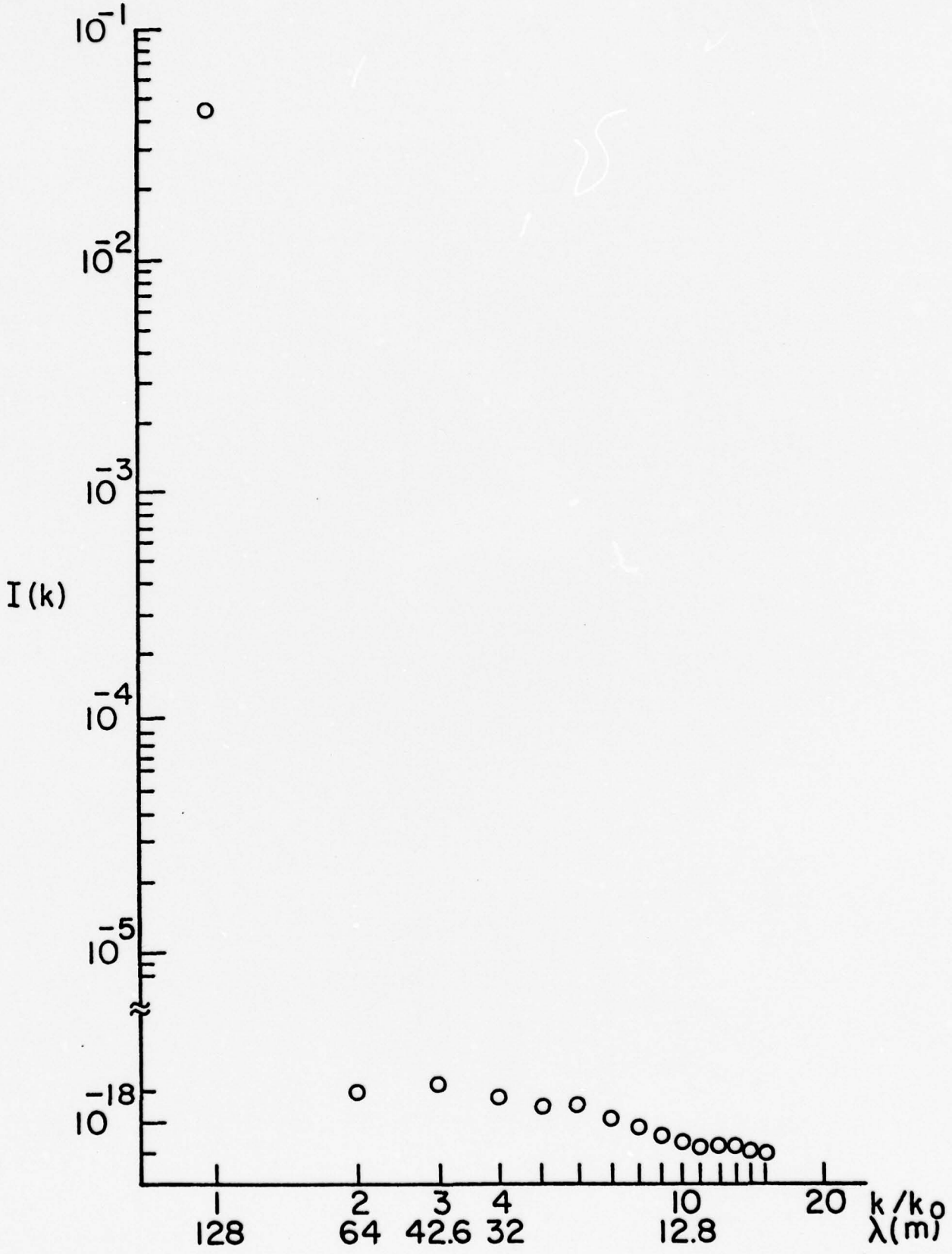
10^{-1}
10^{-2}
10^{-3}
I(k)
10^{-4}
10^{-5}
10^{-18}
1
2
3
4
10
20
k/k₀
128
64
42.6
32
12.8
λ(m)

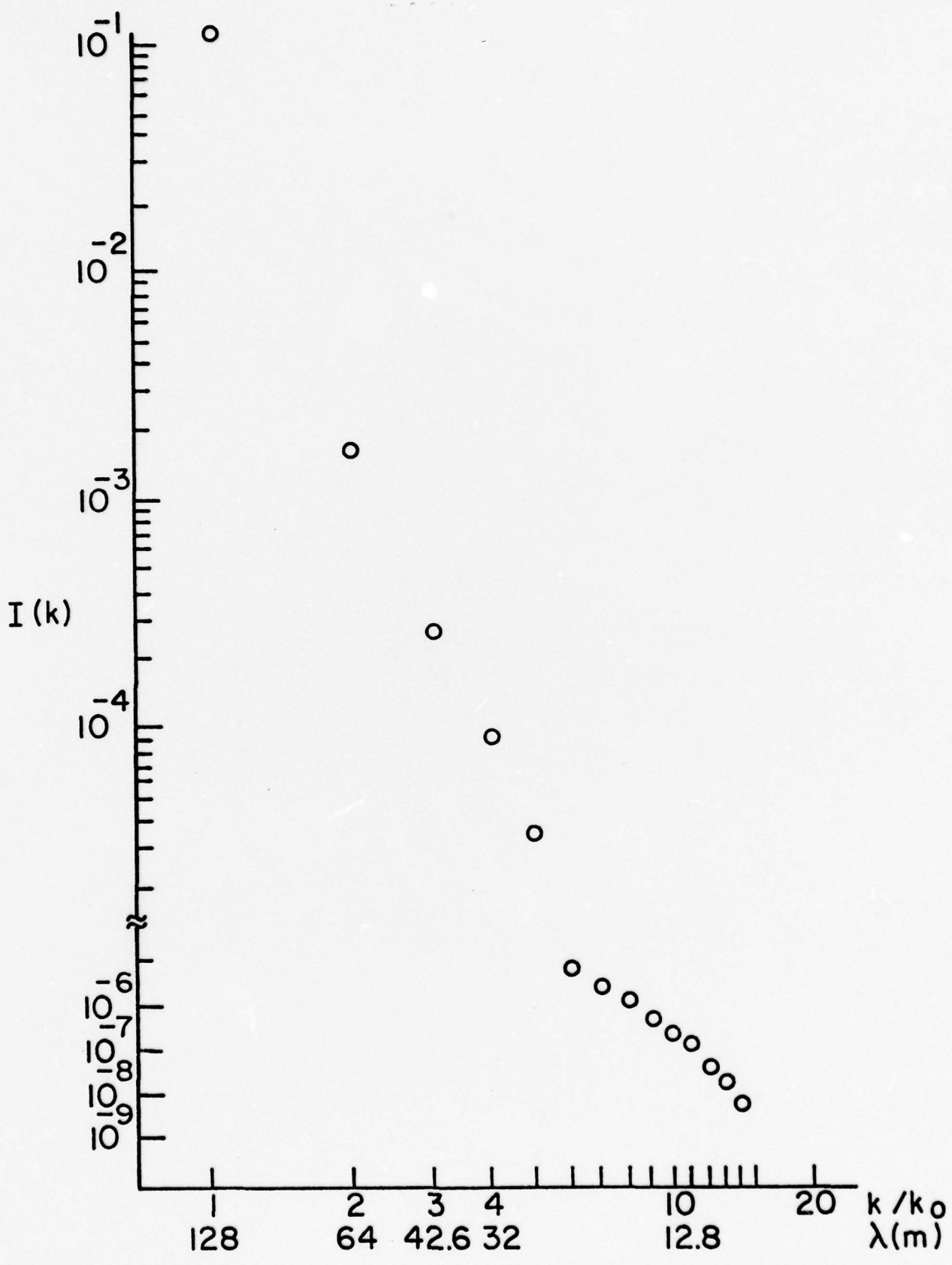
10^{-1}
10^{-2}
10^{-3}
I (k)
10^{-4}
10^{-6}
10^{-7}
10^{-8}
10^{-9}
1
2
3
4
10
20
k /k o
128
64
42.6
32
12.8
λ(m)

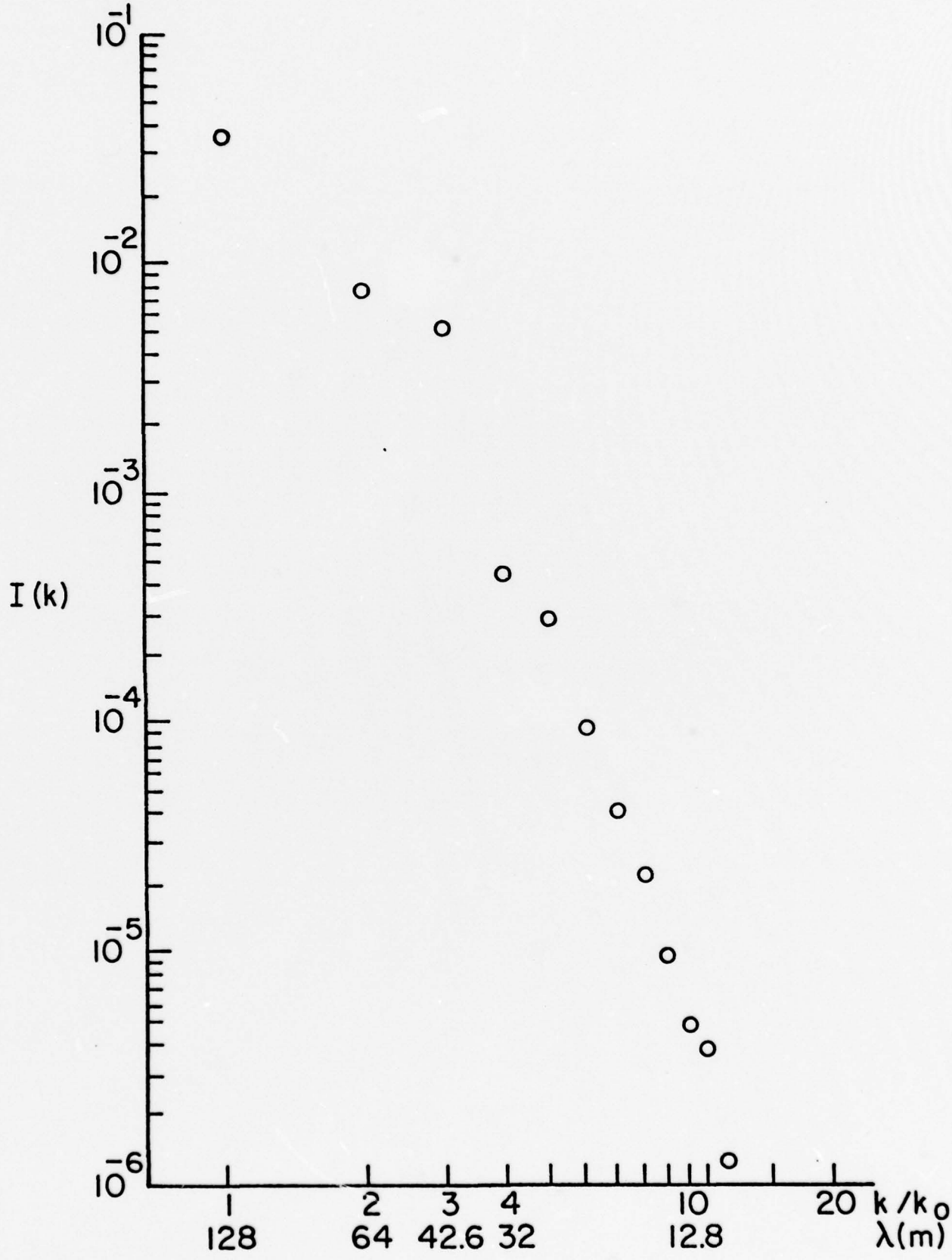
10^{-1}
10^{-2}
10^{-3}
10^{-4}
10^{-5}
10^{-6}
I (k)
1
2
3
4
10
20
k/k_o
128
64
42.6
32
12.8
λ(m)

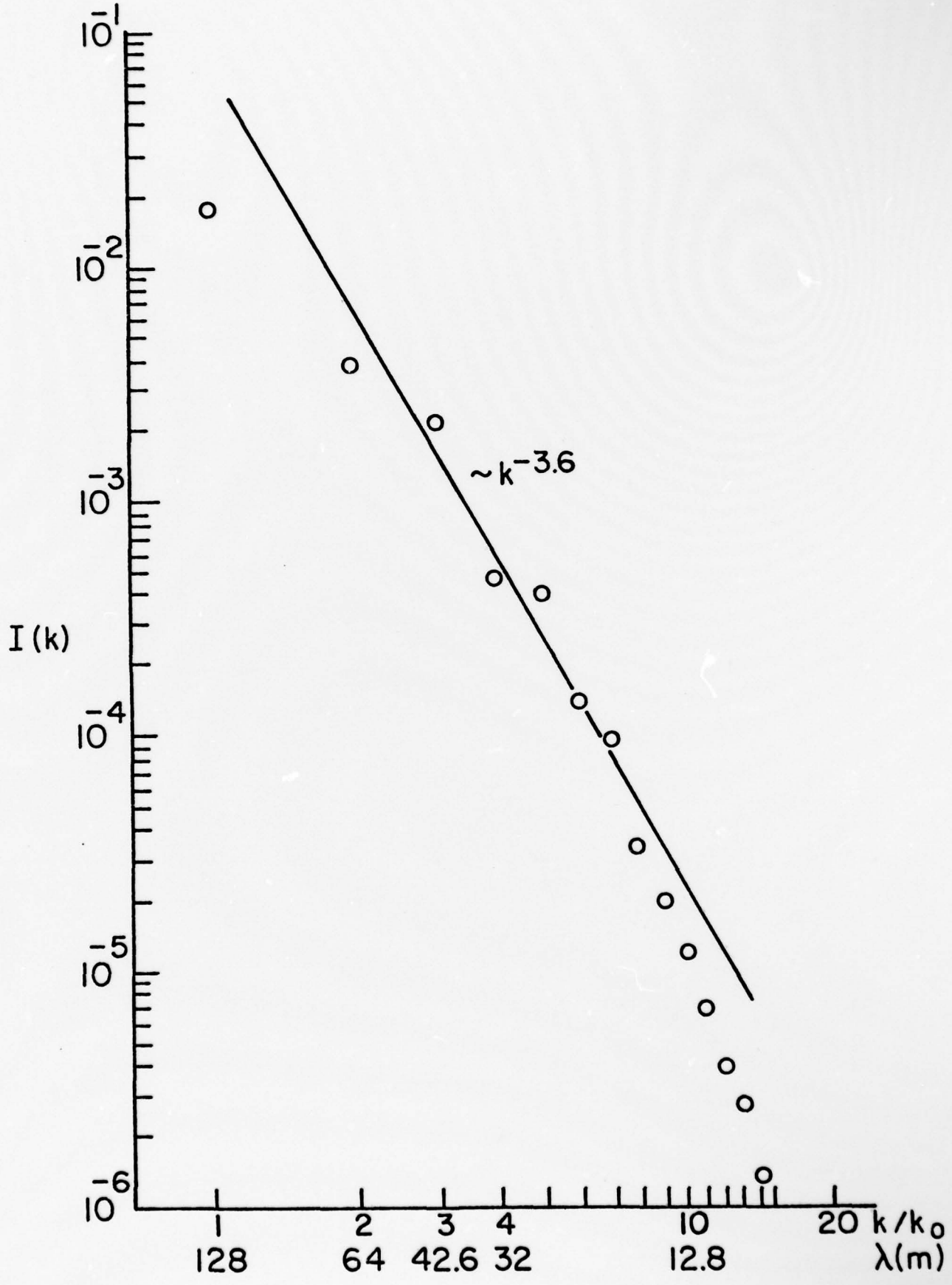
10^{-1}
10^{-2}
10^{-3}
10^{-4}
10^{-5}
10^{-6}
I (k)
$\sim k^{-3.6}$
1
2
3
4
10
20
k/k₀
128
64
42.6
32
12.8
λ(m)

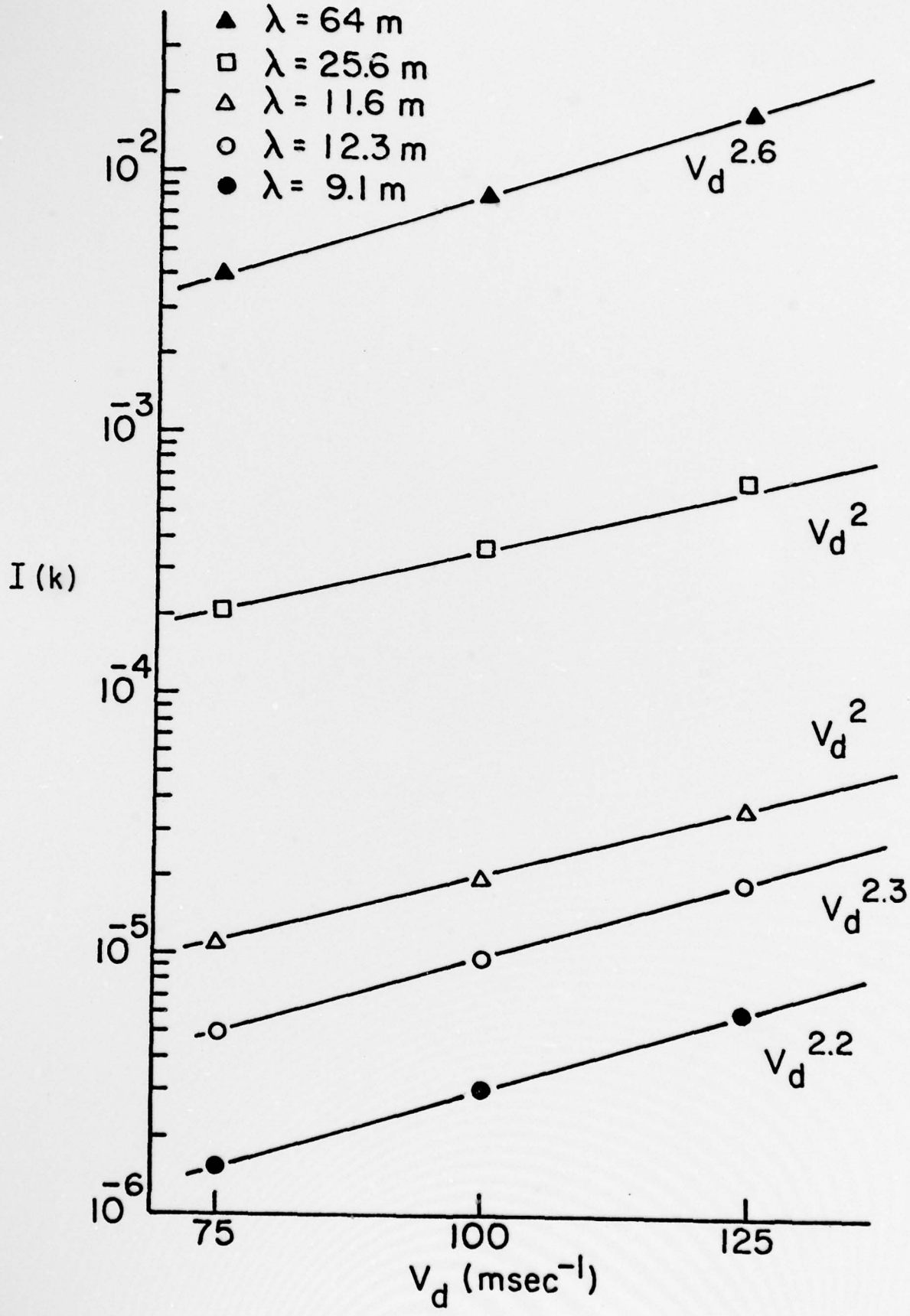
λ = 64 m
λ = 25.6 m
λ = 11.6 m
λ = 12.3 m
λ = 9.1 m
10^{-2}
10^{-3}
10^{-4}
10^{-5}
10^{-6}
I (k)
$V_d^{2.6}$
V_d^{2}
V_d^{2}
$V_d^{2.3}$
$V_d^{2.2}$
75
100
125
V_d (msec^{-1})

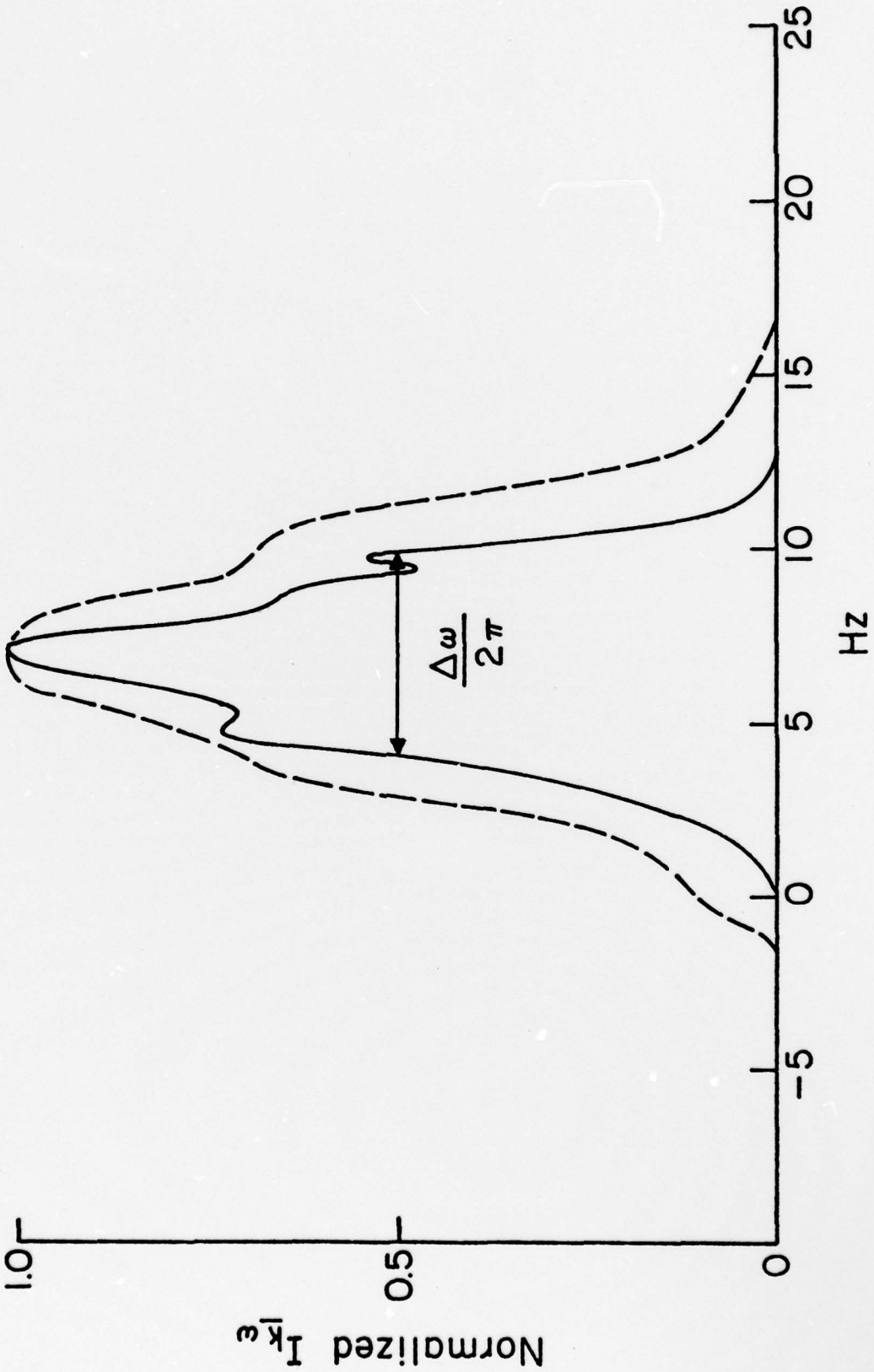
Normalized $I_{k\omega}$
1.0
0.5
0
-5
0
5
10
15
20
25
Hz
$\frac{\Delta\omega}{2\pi}$

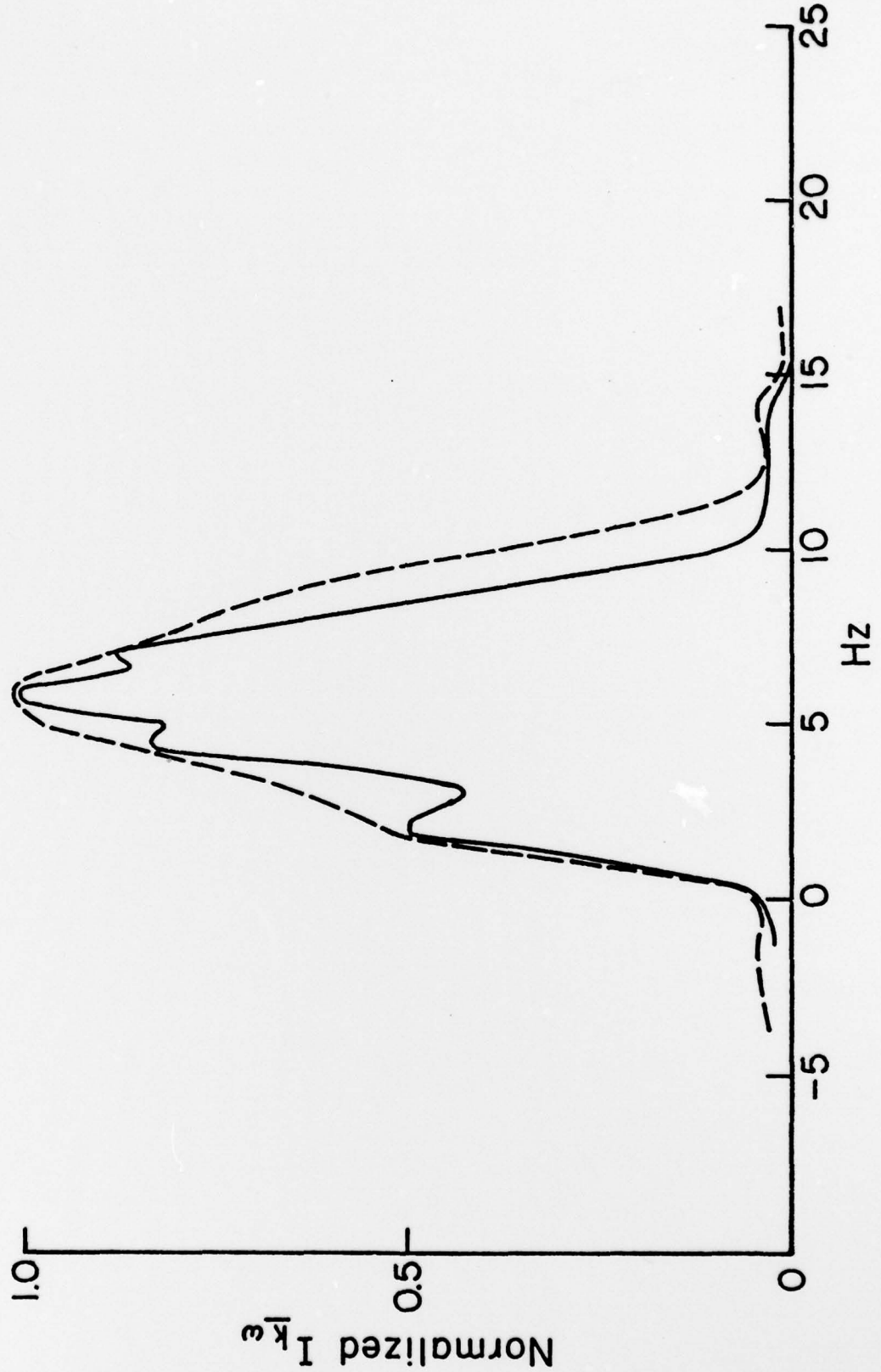
Normalized $I_{k\omega}$
1.0
0.5
0
-5
0
5
10
15
20
25
Hz

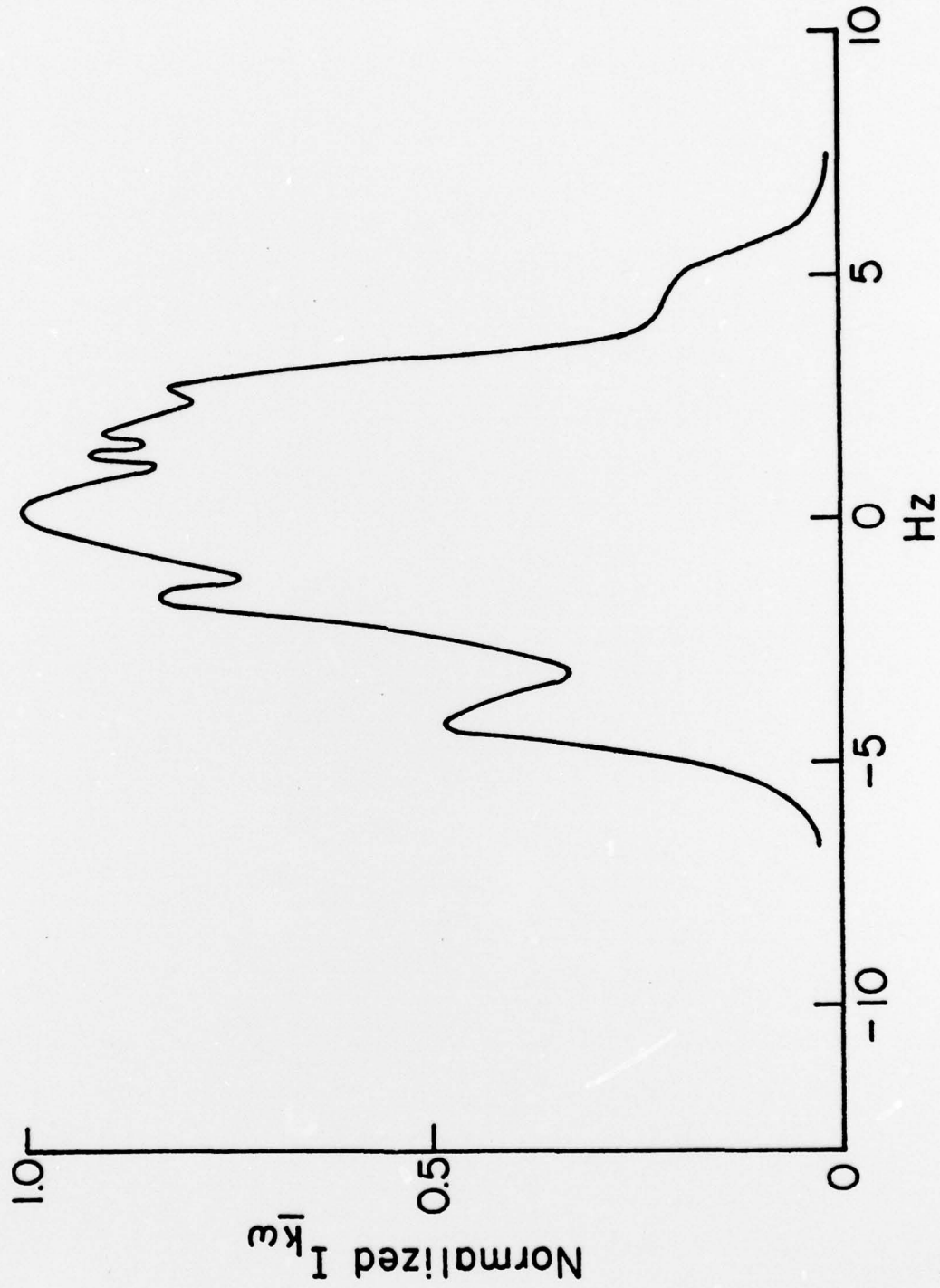
Normalized $I_{\bar{k}\omega}$
1.0
0.5
0
-10
-5
0
5
10
Hz

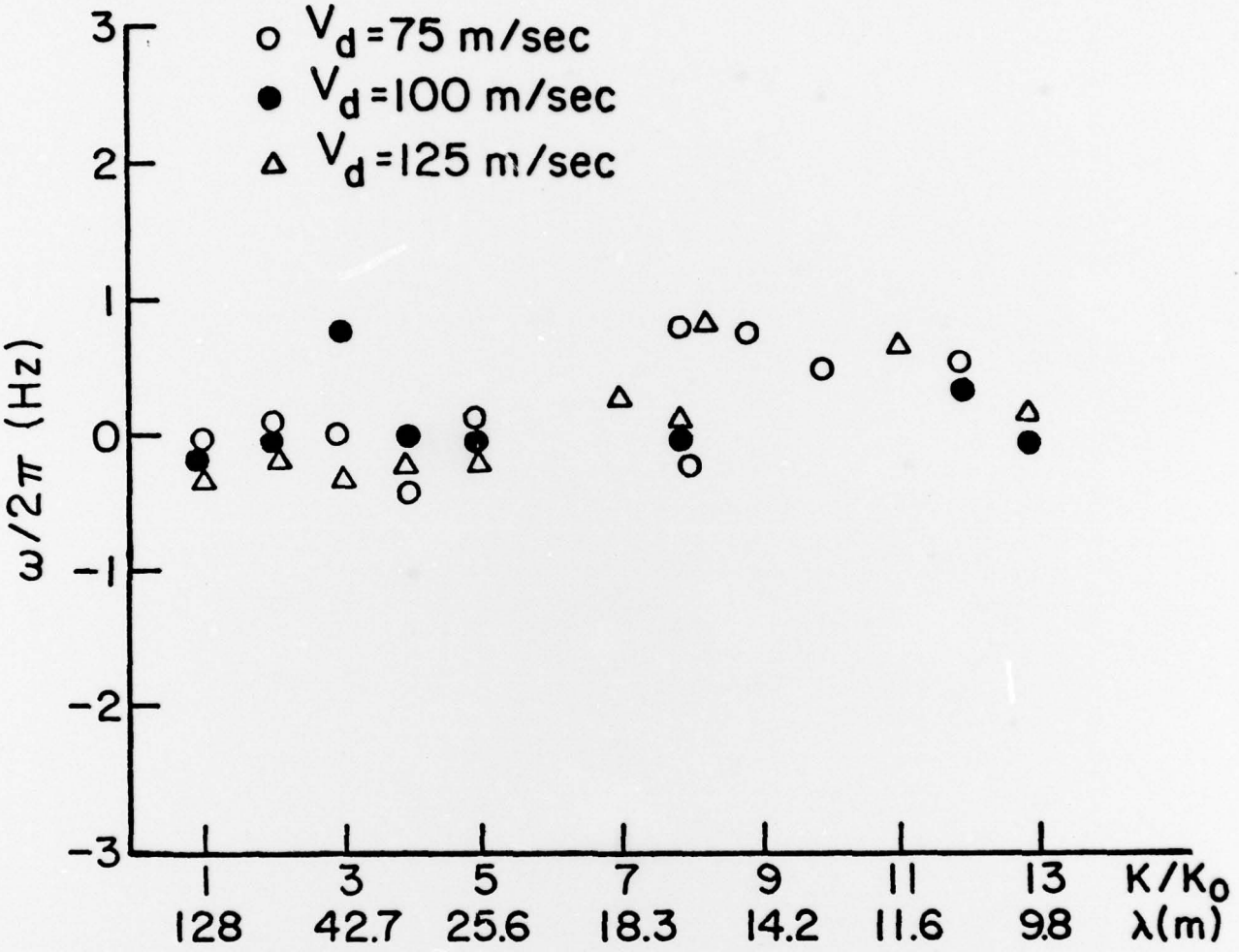
o V_d=75 m/sec
● V_d=100 m/sec
△ V_d=125 m/sec
ω/2π (Hz)
3
2
1
0
-1
-2
-3
1
3
5
7
9
11
13
K/K₀
128
42.7
25.6
18.3
14.2
11.6
9.8
λ(m)

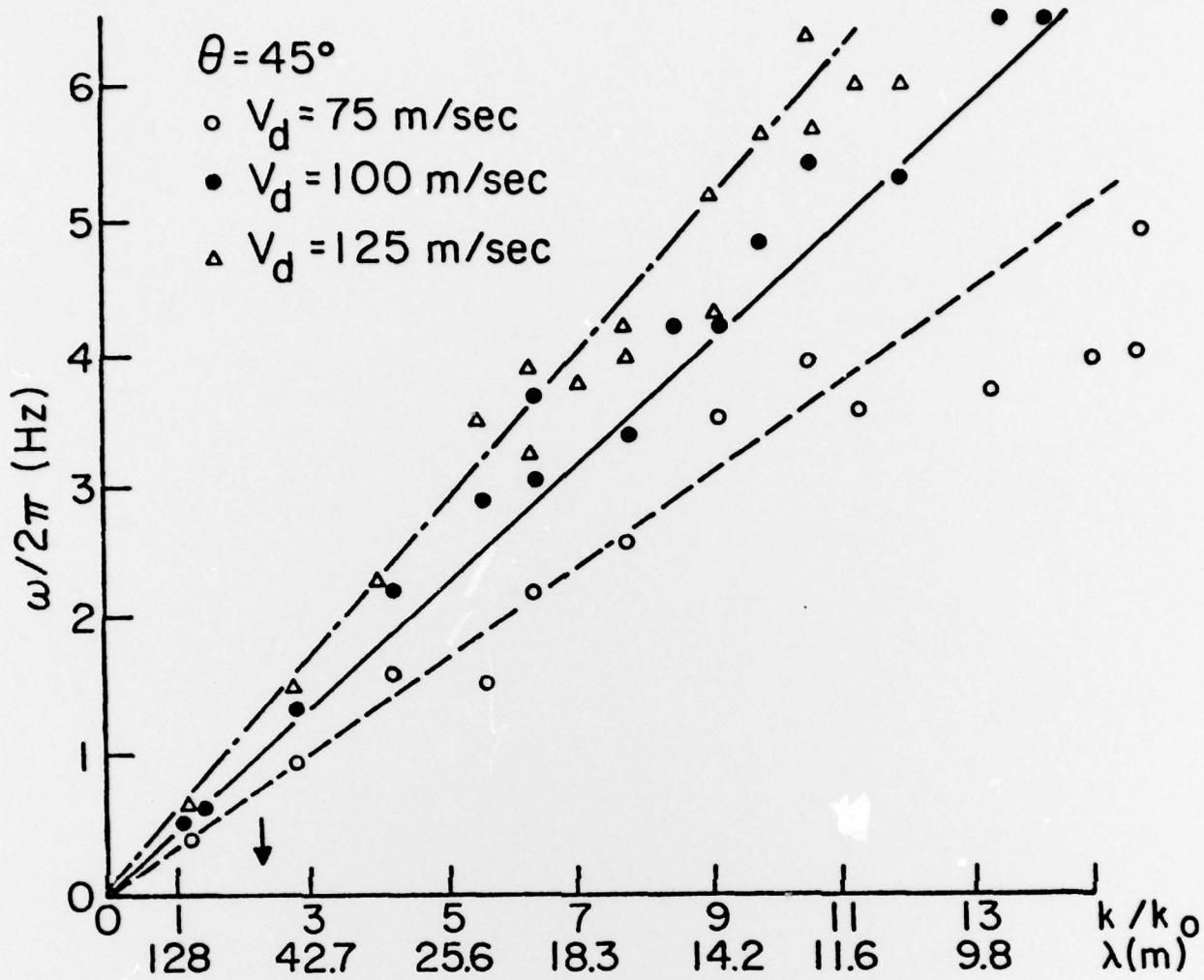
θ = 45°
V_d = 75 m/sec
V_d = 100 m/sec
V_d = 125 m/sec
ω/2π (Hz)
0
1
2
3
4
5
6
0
1
3
5
7
9
11
13
k/k_o
128
42.7
25.6
18.3
14.2
11.6
9.8
λ(m)

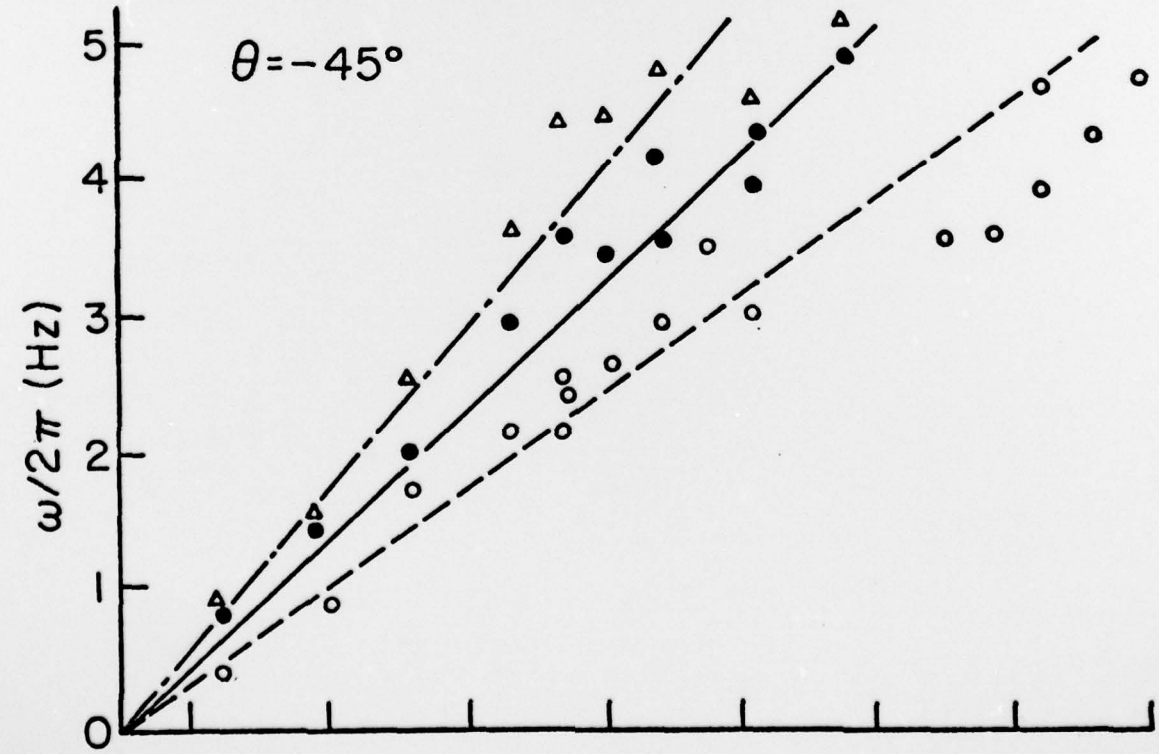
θ = −45°
ω/2π (Hz)
0
1
2
3
4
5

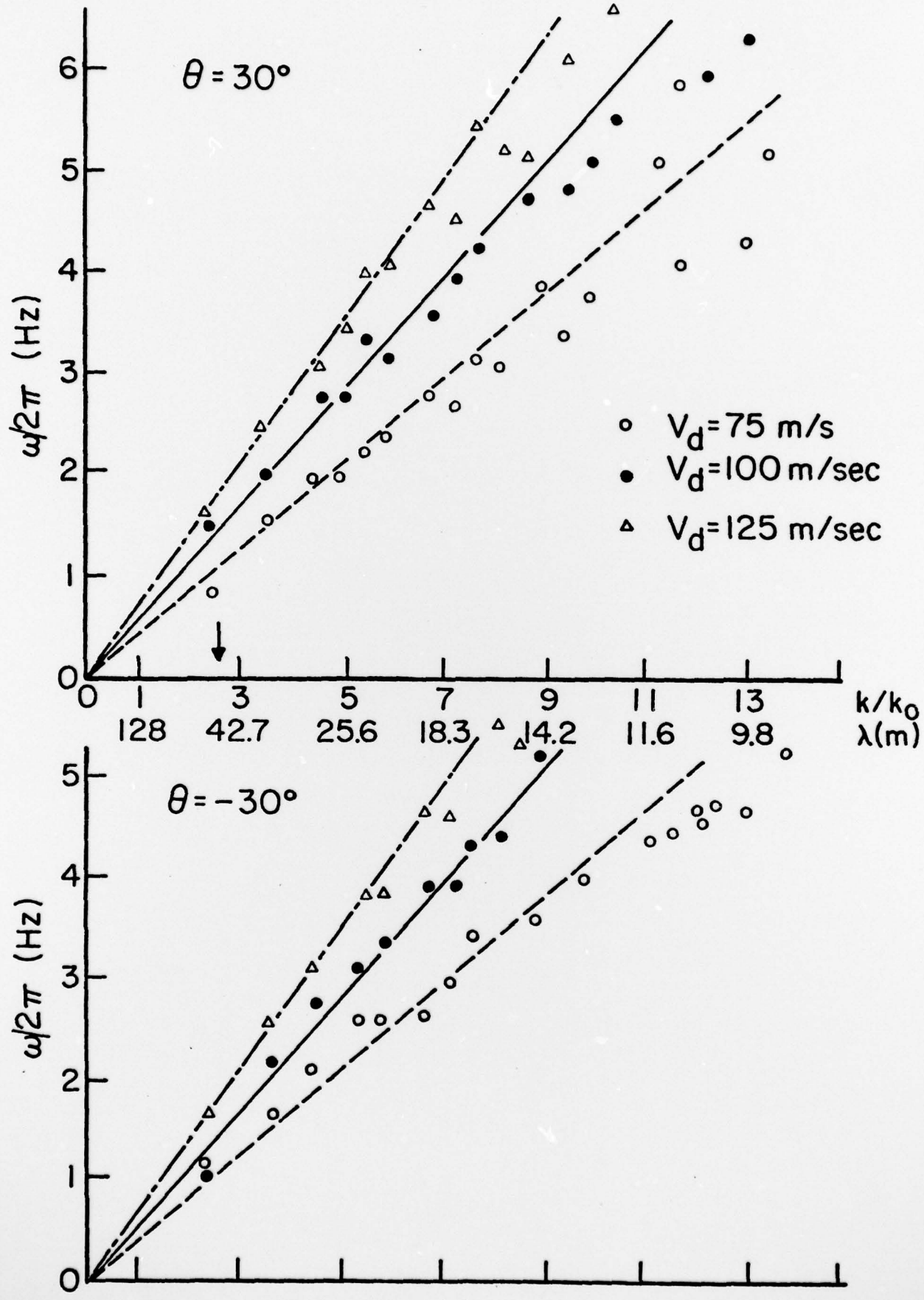
θ = 30°
ω/2π (Hz)
0
1
2
3
4
5
6
V_d = 75 m/s
V_d = 100 m/sec
V_d = 125 m/sec
0 1 3 5 7 9 11 13
k/k₀
128 42.7 25.6 18.3 14.2 11.6 9.8
λ(m)
θ = −30°
ω/2π (Hz)
0
1
2
3
4
5

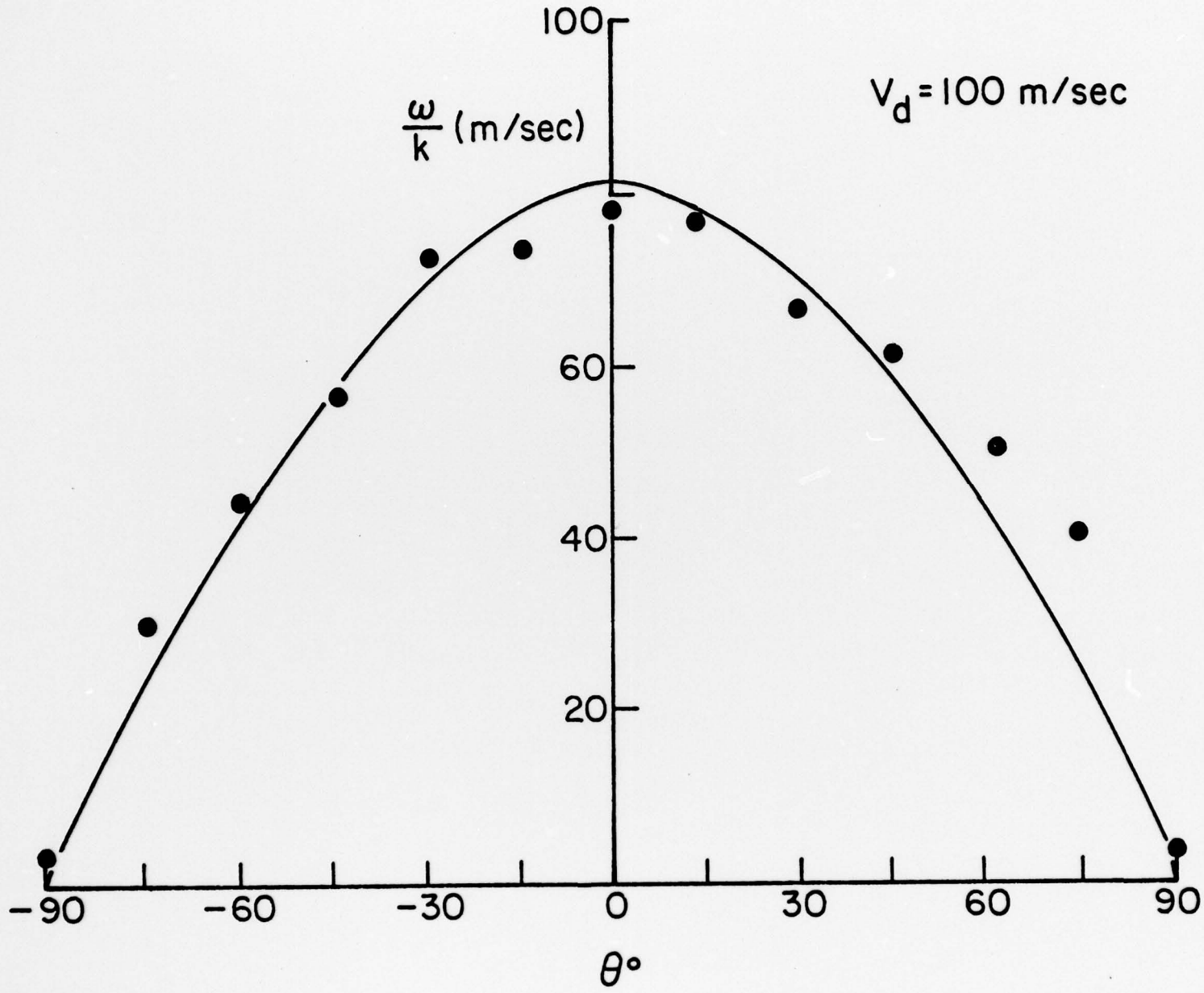
100
60
40
20
$\frac{\omega}{k}$ (m/sec)
V_d = 100 m/sec
-90
-60
-30
0
30
60
90
θ°

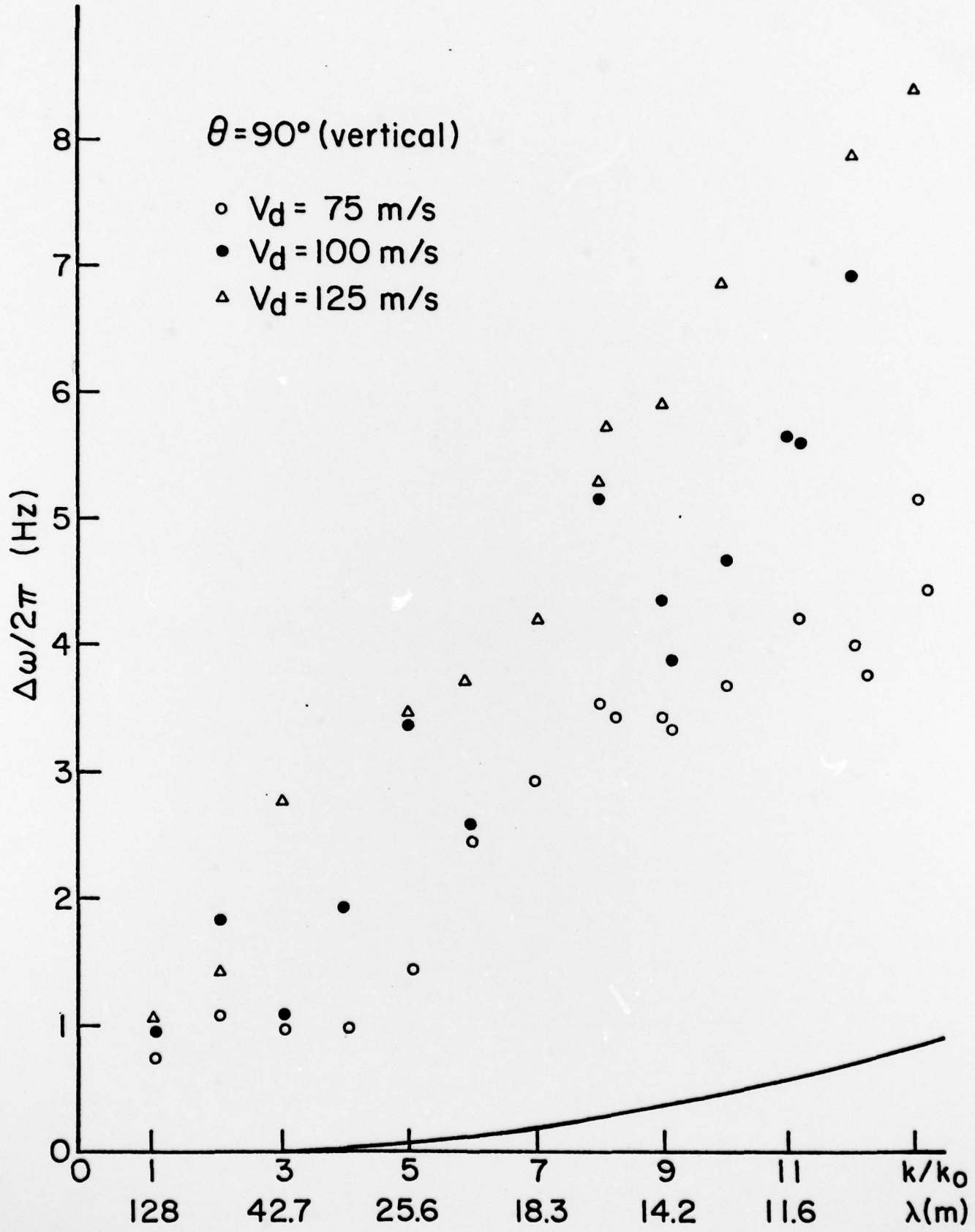
θ = 90° (vertical)
o Vd = 75 m/s
• Vd = 100 m/s
Δ Vd = 125 m/s
Δω/2π (Hz)
0
1
2
3
4
5
6
7
8
0
1
3
5
7
9
11
k/k0
128
42.7
25.6
18.3
14.2
11.6
λ(m)

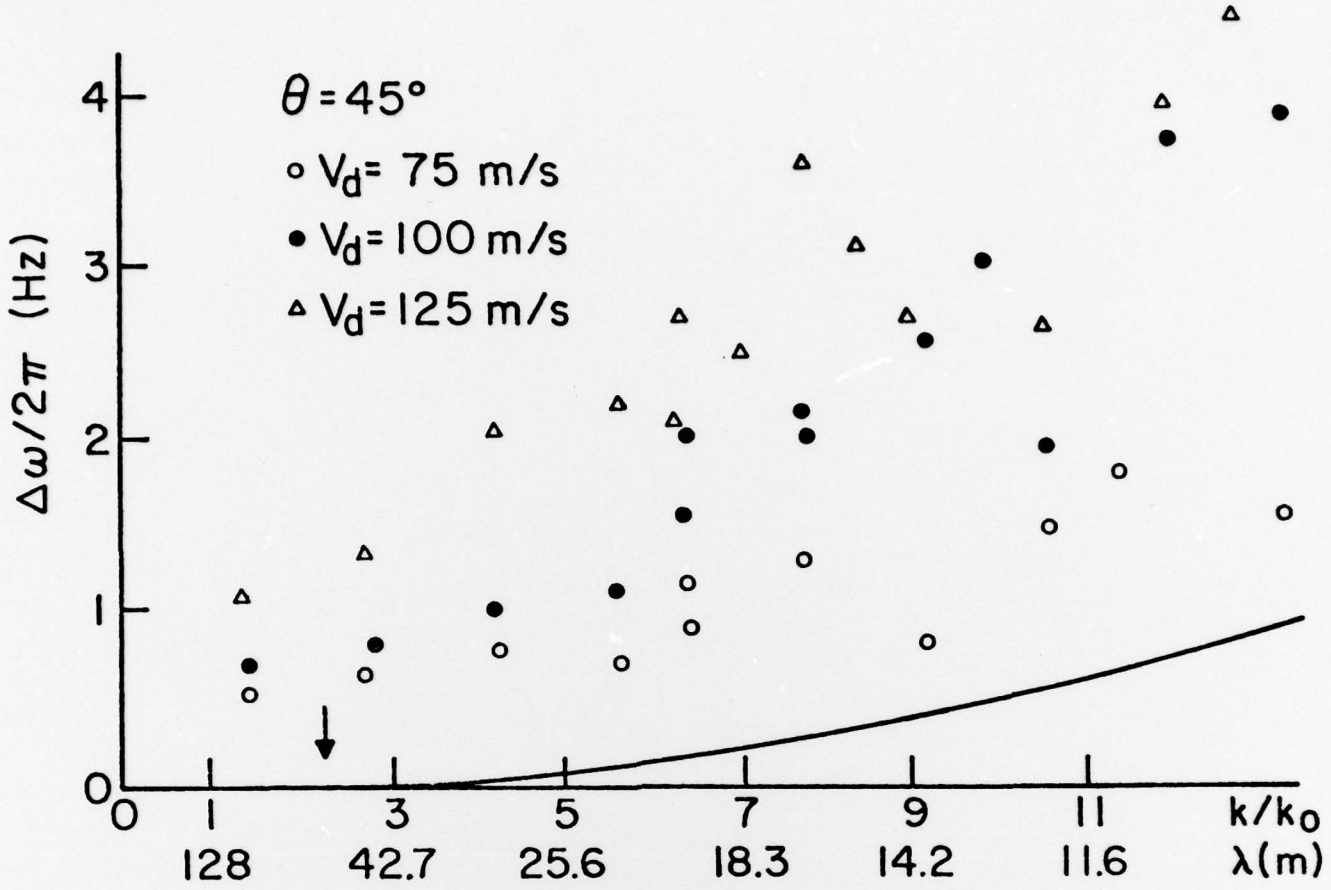
θ = 45°
○ V_d = 75 m/s
● V_d = 100 m/s
△ V_d = 125 m/s
Δω/2π (Hz)
0
1
2
3
4
0
1
3
5
7
9
11
k/k₀
128
42.7
25.6
18.3
14.2
11.6
λ(m)

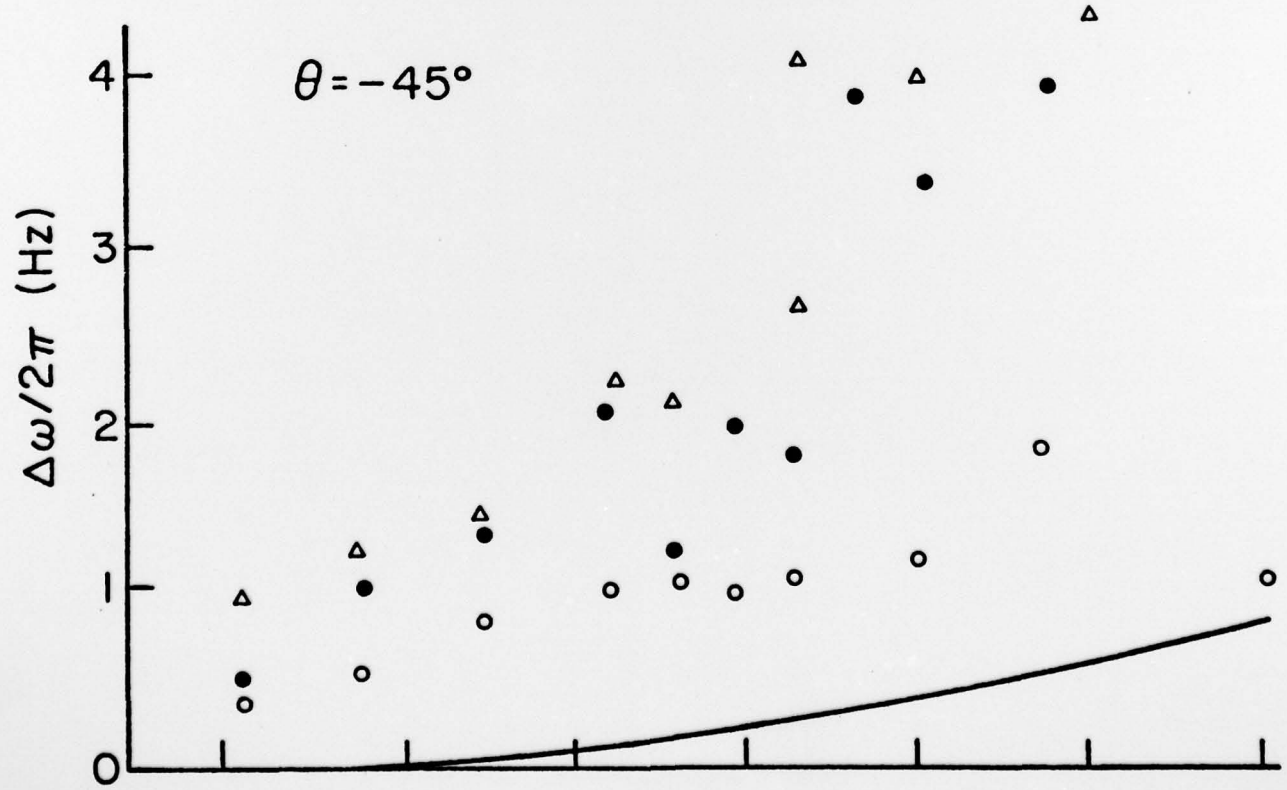
θ = −45°
Δω/2π (Hz)
0
1
2
3
4

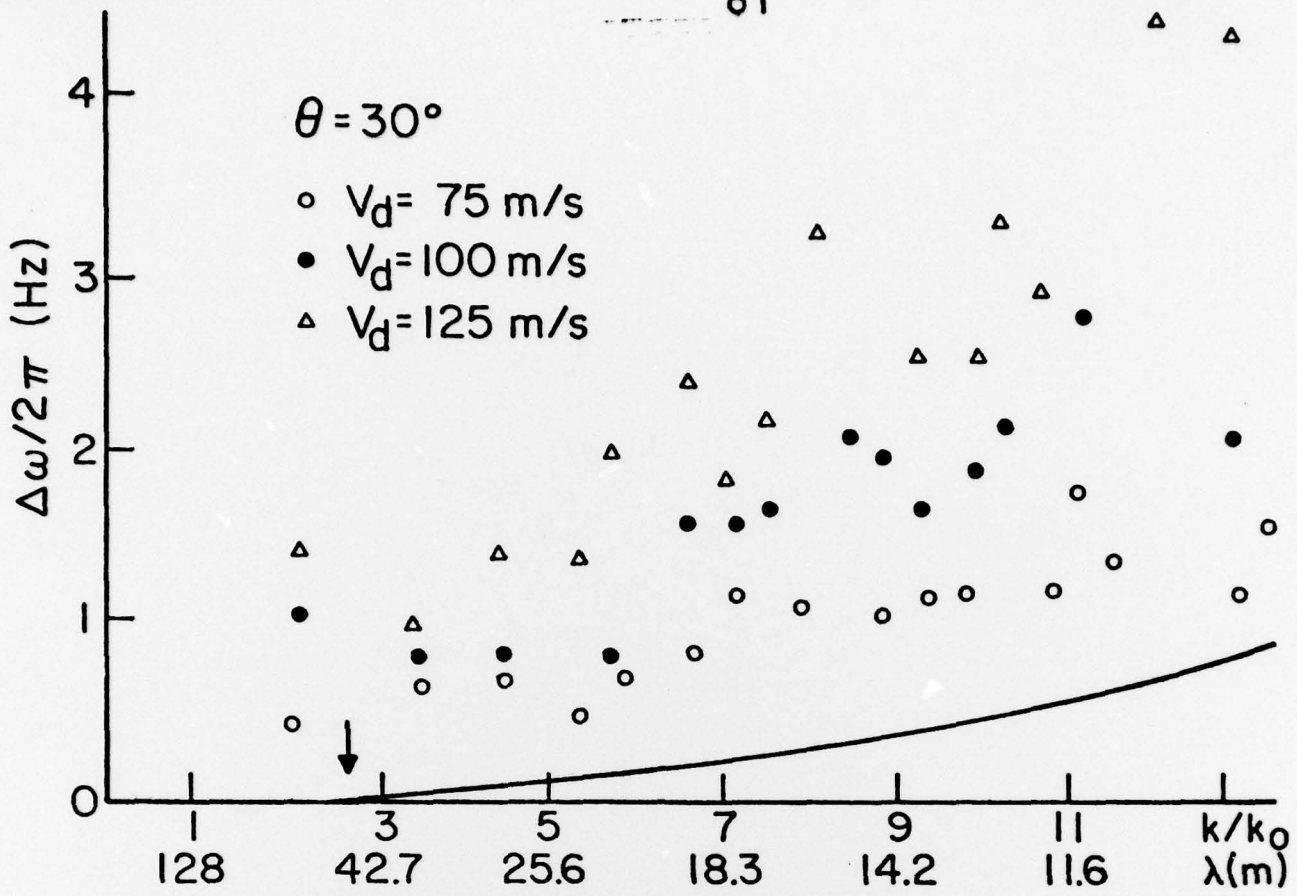
θ = 30°
○ V_d = 75 m/s
● V_d = 100 m/s
△ V_d = 125 m/s
Δω/2π (Hz)
0
1
2
3
4
1
3
5
7
9
11
k/k0
128
42.7
25.6
18.3
14.2
11.6
λ(m)

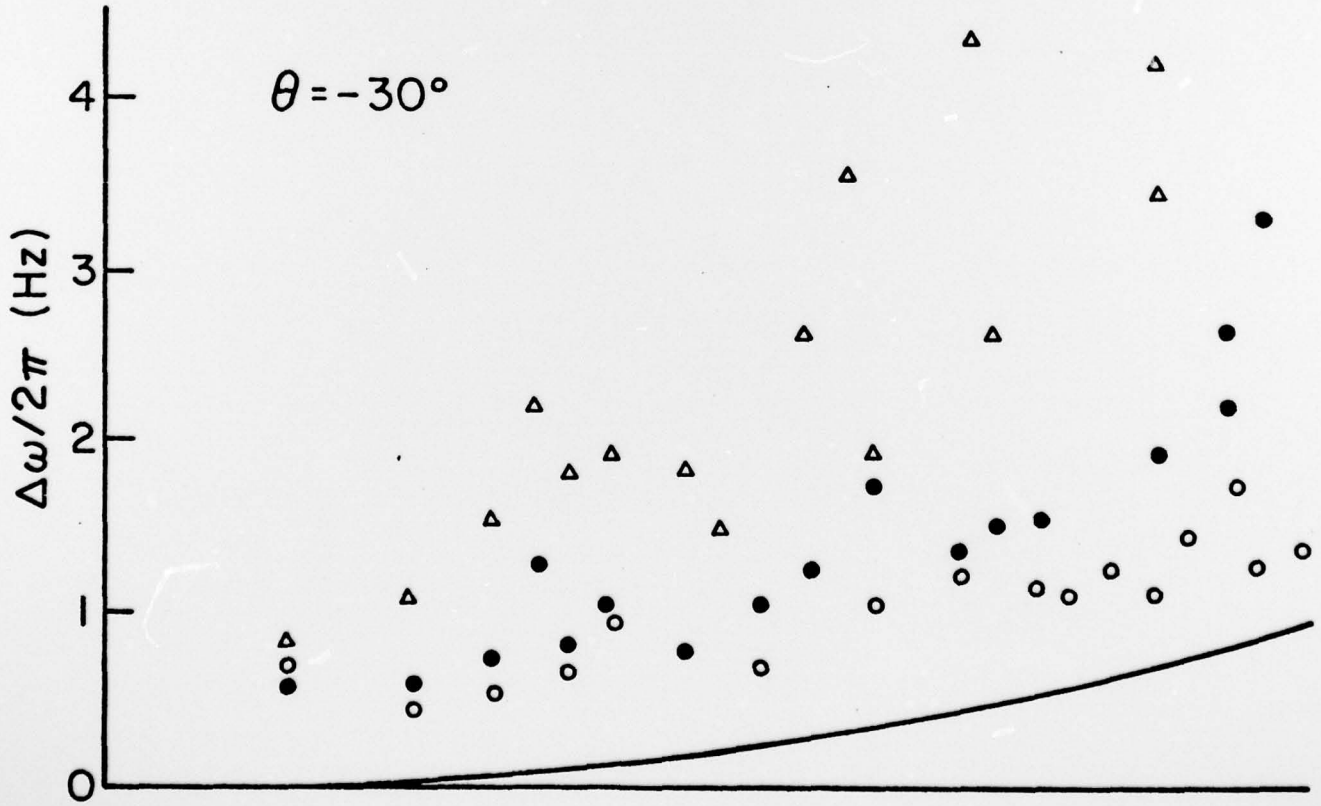
θ = -30°
Δω/2π (Hz)
0
1
2
3
4

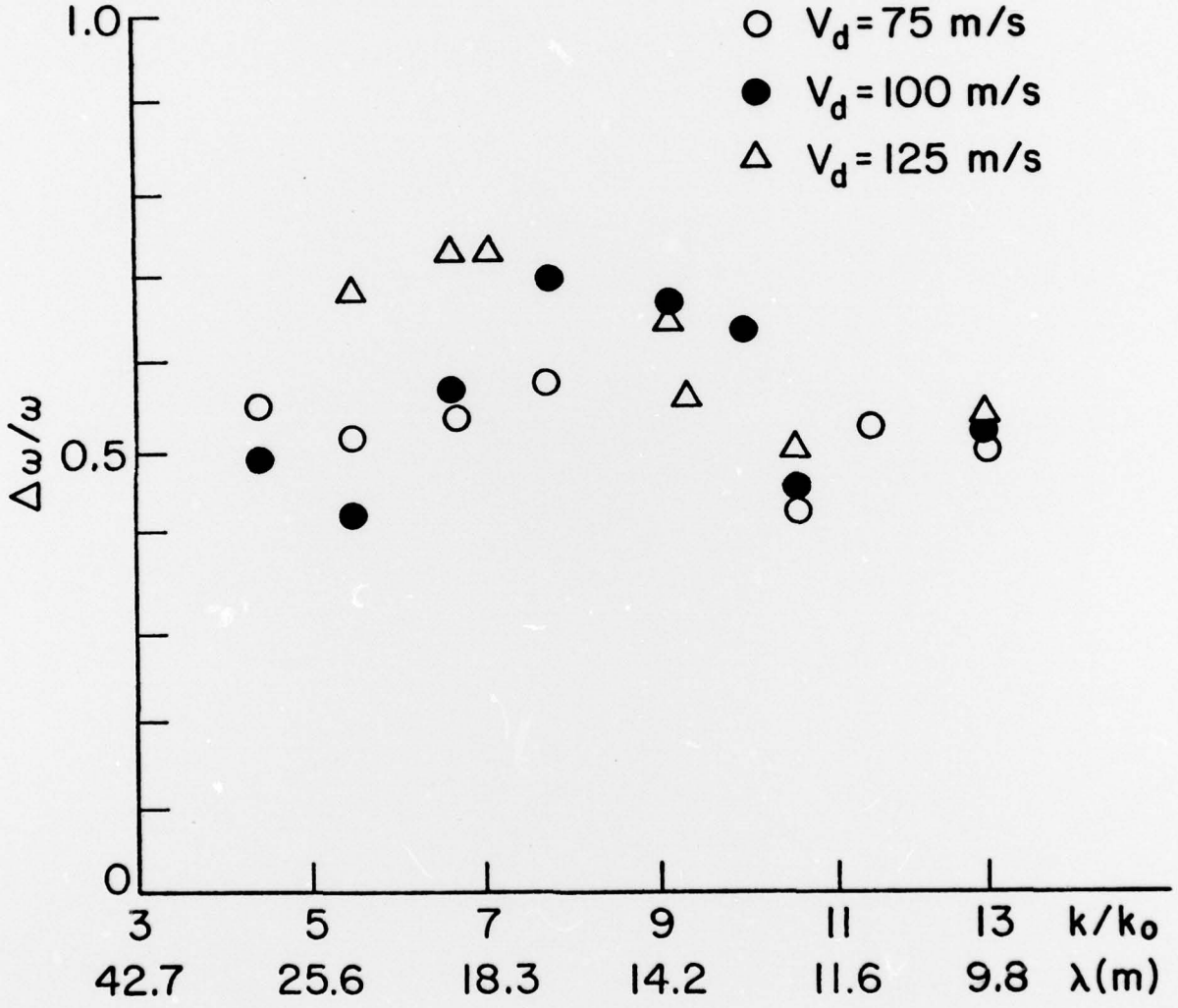
1.0
0.5
0
Δω/ω
○ V_d = 75 m/s
● V_d = 100 m/s
△ V_d = 125 m/s
3
5
7
9
11
13
k/k₀
42.7
25.6
18.3
14.2
11.6
9.8
λ(m)

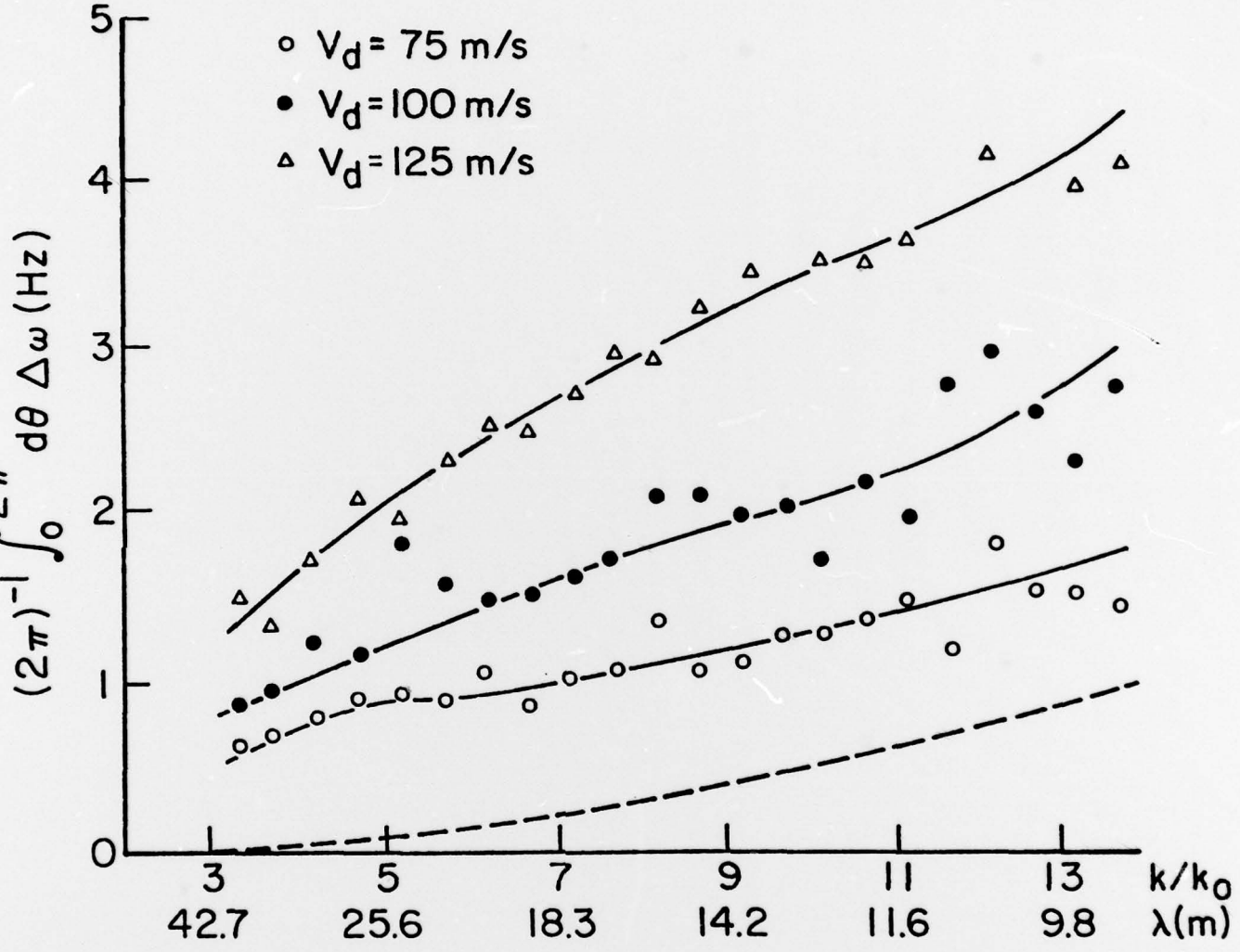
V_d = 75 m/s
V_d = 100 m/s
V_d = 125 m/s
$(2\pi)^{-1}\int_0^{2\pi} d\theta\, \Delta\omega$ (Hz)
0
1
2
3
4
5
3
5
7
9
11
13
k/k_0
42.7
25.6
18.3
14.2
11.6
9.8
λ(m)

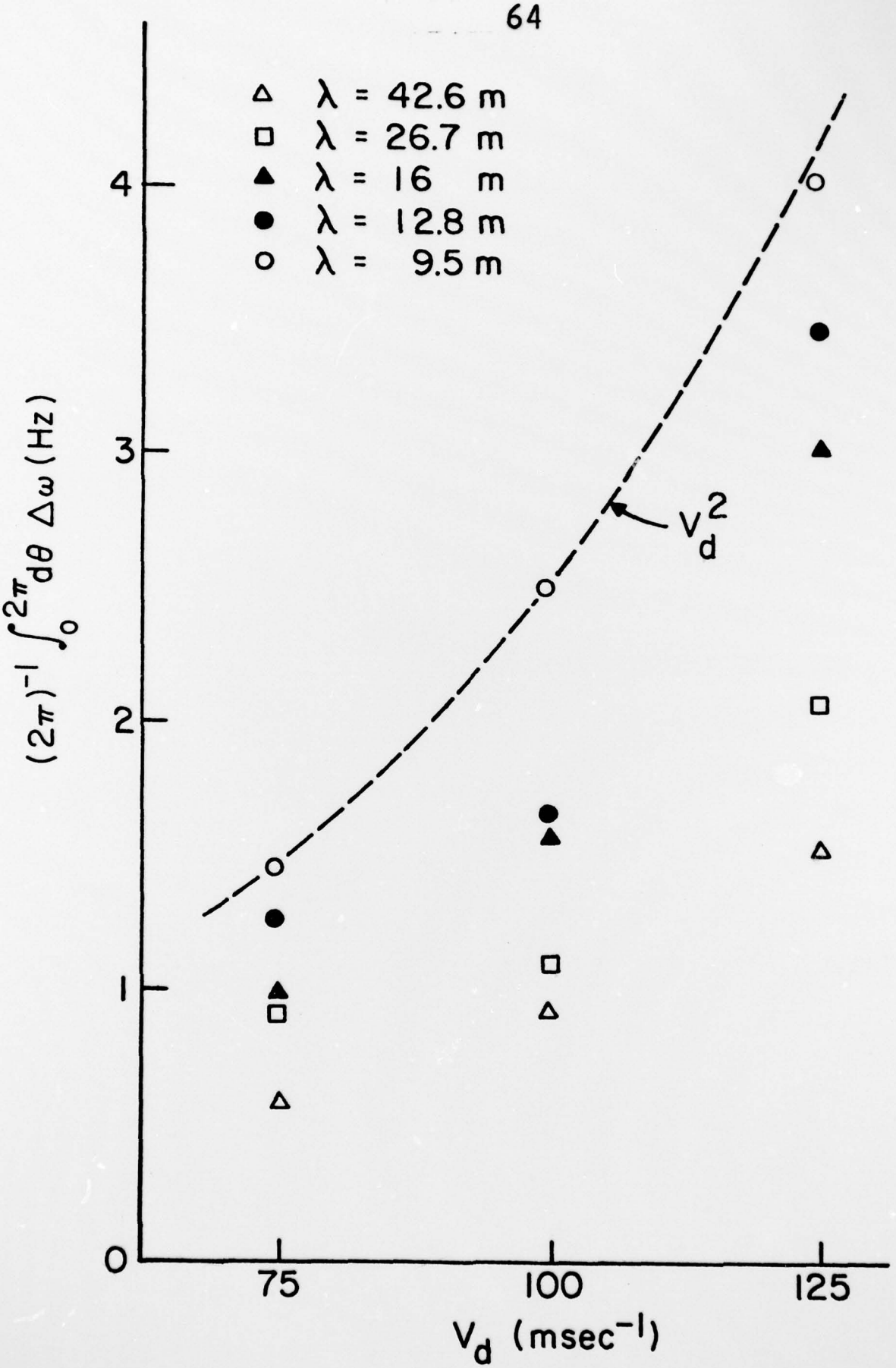
λ = 42.6 m
λ = 26.7 m
λ = 16 m
λ = 12.8 m
λ = 9.5 m
V_d^2
$(2\pi)^{-1} \int_0^{2\pi} d\theta \, \Delta\omega$ (Hz)
V_d (msec^{-1})
0
1
2
3
4
75
100
125

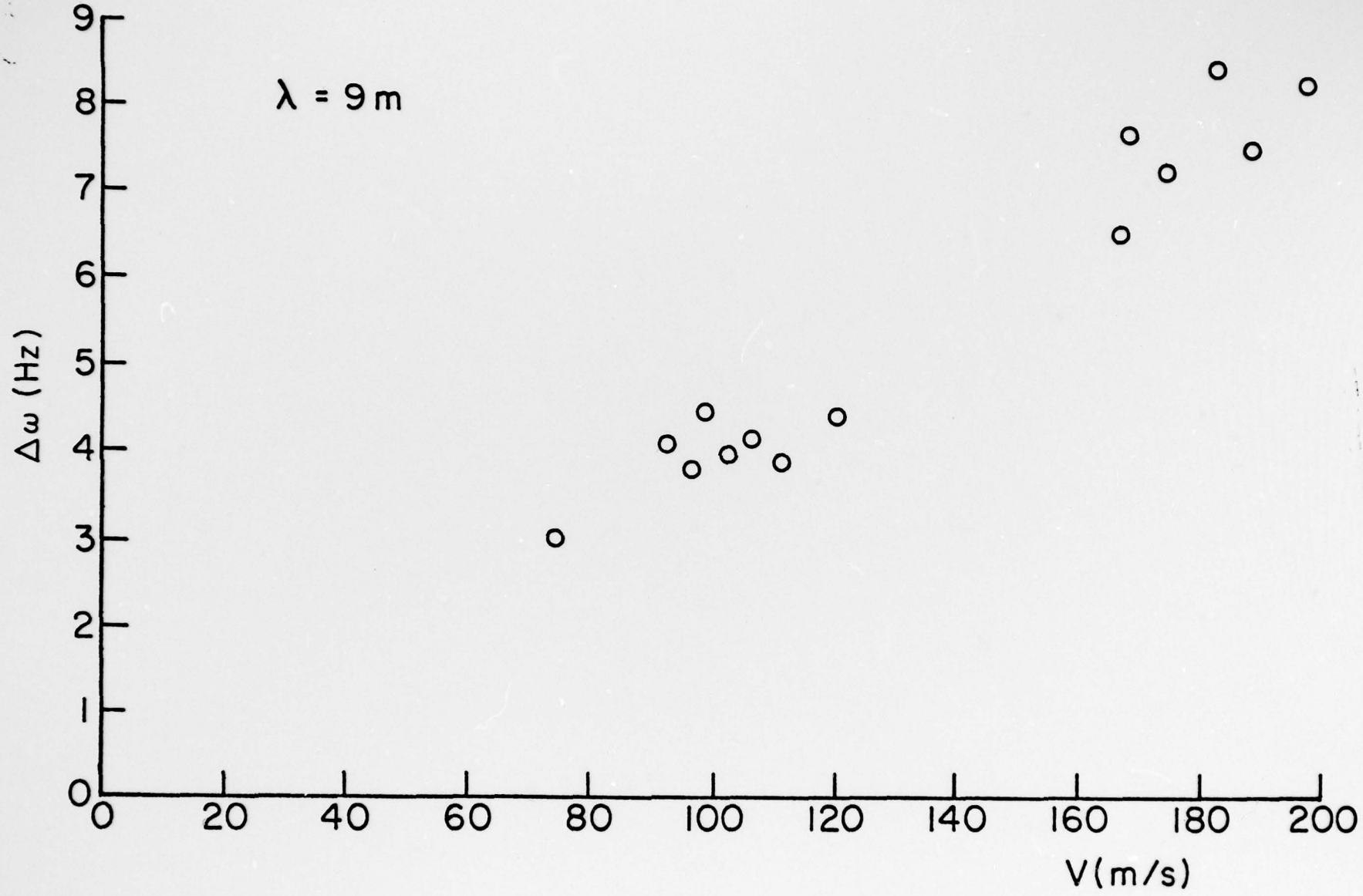
λ = 9 m
Δω (Hz)
V(m/s)
0
1
2
3
4
5
6
7
8
9
0
20
40
60
80
100
120
140
160
180
200

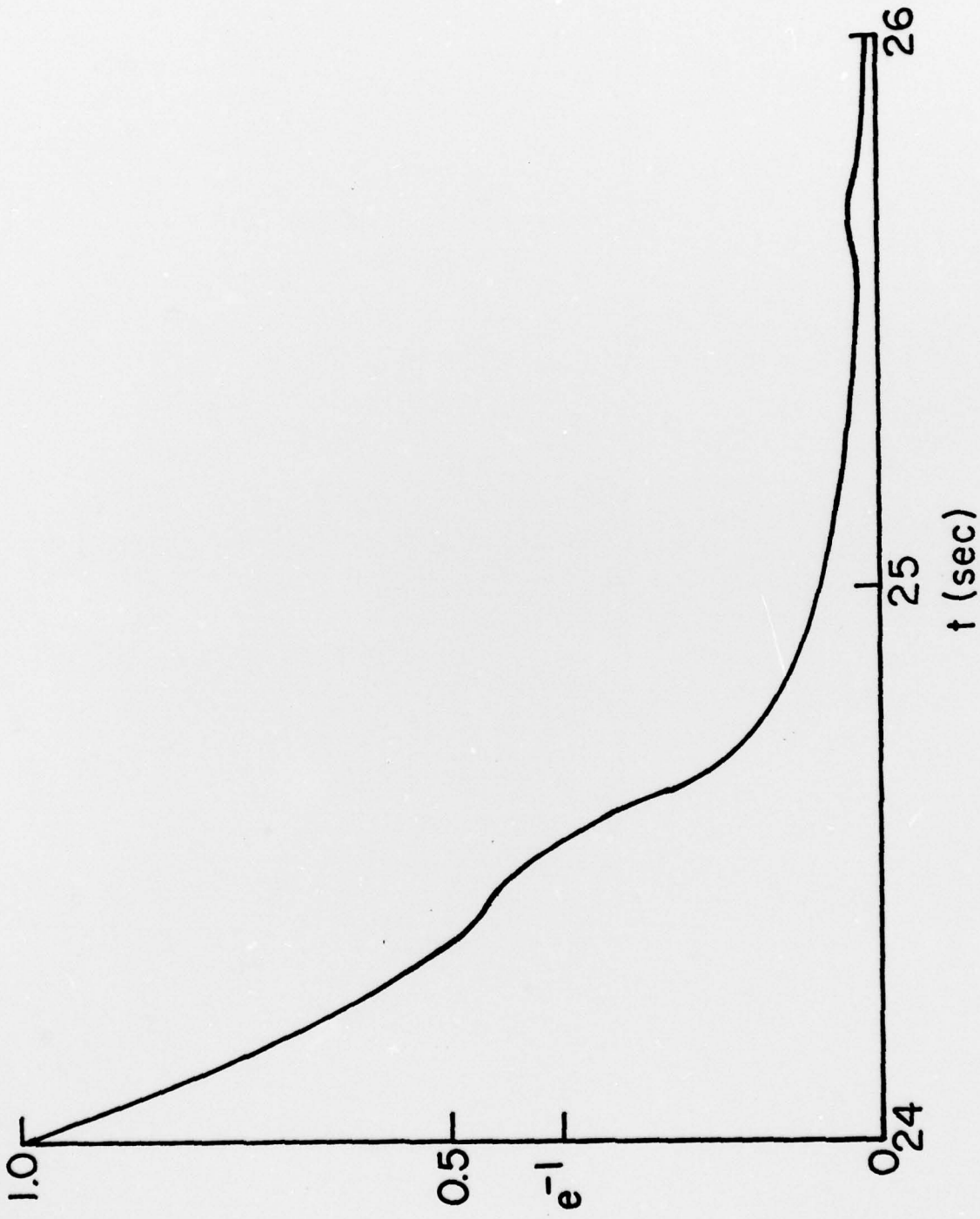
1.0
0.5
e^{-1}
0
24
25
26
t (sec)